Rochester Institute of Technology

RIT Digital Institutional Repository

Theses

2005

Al2O3 hosted attenuated phase shift mask materials for 157 nm

Yang Liu

Follow this and additional works at: https://repository.rit.edu/theses

Recommended Citation

Liu, Yang, "Al2O3 hosted attenuated phase shift mask materials for 157 nm" (2005). Thesis. Rochester Institute of Technology. Accessed from

This Thesis is brought to you for free and open access by the RIT Libraries. For more information, please contact repository@rit.edu.

Master of Science in Materials Science and Engineering

Al_2O_3 Hosted Attenuated Phase Shift Mask Materials for 157 nm

By Yang Liu

Submitted in Fulfillment of the Requirements for the Degree of Master of Science

Approved:

Bruce W. Smith

Thesis Advisor

K.S.V. Santhanam

Department Head

Department of Materials Science and Engineering
Rochester Institute of Technology
Rochester, New York

Jan 18 2005

I, Yang Liu, welcome and authorize anybody to photocopy or reproduce all or any part of my print thesis.

Author: Yang Liu
Date: Jan 18 2005

Table of Contents

Table of contents....i

List of figures....iii

List of tables....v

Acknowledgements....vi

Abstract....1

1. Introduction....3
   1.1 Background and technology trend....3

2. Theory....13
   2.1 Parameters of *APSM*....13
   2.2 Materials screening for *APSM*....15
   2.3 Consideration of *APSM* at 157nm....16
   2.4 Modeling....17
   2.5 Modeling of thin film optical properties....21
   2.6 Photoresist patterning: lift-off process....24

3. Experimental....27
   3.1 Thin film deposition....27
   3.2 Determination of n and k of thin film....31
      3.2.1 Ellipsometry....31
      3.3.2 Ellipsometer measuring process....32
   3.3 Lift-off process....35
      3.3.1 Process consideration....35
      3.3.2 Image reversal process....37
      3.3.3 Processing and analysis....38

4. Results....46

4.1 Candidate films.......46

4.1.1 *Al-NbO*$_x$.......46

4.2.2 *Al-TaO*$_x$.......52

4.1.3 *Al-CrOx*.......59

4.1.4 *Al-MoO*$_x$.......61

4.2 Lift-Off.......63

5.Conclusion.......66

6. References.......69

7. Abbreviations.......71

List of figures

Figure 1.1 Moore's law and the future of lithography...4
Figure 1.2. Microlithography goes to sub-wavelength...5
Figure 1.3. Critical Dimension vs. Numerical Aperture for different wavelengths.........7
Figure 1.4. Depth of focus vs. Numerical Aperture for different wavelengths..............8
Figure 1.5. Comparison between Binary Mask and *APSM*.....................................10
Figure 1.6. The 0th, 1st and 2nd diffraction order values for *APSM* transmission between 0% (binary mask) and 20% with 2% increments...12
Figure 2.1.Diagram of materials refractive index and extinction coefficient diagram at 157 nm..15
Figure 2.2. n and k effect on reflectance..17
Figure 3.1. Illustration of PE2400A RF sputter system...29
Figure3 2. The film composition as a function of N_2 in DC reactive sputtering of *Ta*....30
Figure 3.3. A schematic diagram of a nulling ellipsometer setup............................32
Figure 3.4. J.A. Woollam WVASE spectroscopic ellipsometer................................33
Figure 3.5. Data analysis flow chart...34
Figure 3.6 Image Reversal Lift-Off process flow chart...38
Figure 3.7 AZ5214E coating thickness vs. Spinner speed.....................................39
Figure 3.8 AZ5214E diluted with AZ1500 thinner coating thickness vs. Spinner speed.39
Figure 3.9 Cross section of photoresist profile during exposure and after development..42
Figure.3.10 Cross-section profile after PVD thermal process................................43
Figure 4.1 NbO_x complex index from EMA model...47
Figure 4.2 $Al\text{-}NbO_x$ complex index from EMA model.....................................47
Figure 4.3 Transmission of $Al\text{-}NbO_x$ thin film by simulation based on EMA model......47
Figure 4.4 $Al\text{-}NbO_x$ complex index from measurement....................................48
Figure 4.5 Comparison between modeling prediction and real transmission dispersion of $Al\text{-}NbO_x$..48
Figure 4.6 Phase shift dispersion chart for *Al-NbOx* film before thickness modification.49
Figure 4.7 Phase shift for $Al\text{-}NbO_x$ film after thickness modification.......................50
Figure 4.8 Transmission dispersion chart for $Al\text{-}NbO_x$...50
Figure 4.9 Comparison between EMA model generated data and real data for transmission dispersion...51
Figure 4.10 TaO_x complex index from EMA model...52
Figure 4.11 Al_2O_3 complex index from EMA model...53
Figure 4.12 Transmission of $Al\text{-}TaO_x$ thin film by simulation based on EMA model......53
Figure 4.13 Voltage VS. Power for TaO_x...54
Figure 4.14 Voltage VS. Power for Al_2O_3...54
Figure 4.15 Ellipsometry analysis software fit chart for fabricated $Al\text{-}TaO_x$ thin film.....57
Figure 4.16 Phase shift dispersion chart for *Al-NbOx* film.....................................57
Figure 4.17 Transmission dispersion chart for *Al-TaOx*...57
Figure 4.18 $Al\text{-}TaO_x$ complex index from measurement....................................58
Figure 4.19 Al_2O_3 complex index from EMA model..60
Figure 4.20 CrO_x complex index from EMA model...60
Figure 4.21 $Al\text{-}CrO_x$ complex index from EMA model.....................................60

Figure 4.22 Transmission of $Al\text{-}CrO_x$ thin film by simulation based on EMA model......61
Figure 4.23 MoO_x complex index from EMA model...62
Figure 4.24 $Al\text{-}MoO_x$ complex index from EMA model.......................................63
Figure 4.25 Transmission dispersion chart for $Al\text{-}MoO_x$.......................................63
Figure 4.26 Condition.1: 115C° PEB/0.1 second of exposure...................................64
Figure 4.27 Condition.2: 125C° PEB/0.5 second of exposure...................................64
Figure 4.28 Condition.3: 120C° PEB/0.3 second of exposure...................................64
Figure 4.29 Condition.4: 120C° PEB/0.2 second of exposure...................................64
Figure 4.30 Condition.5: 115C° PEB/0.3 second of exposure...................................65
Figure 4.31 SEM picture of cleaved pattered *APSM* film by Image reversal process......65
Figure 4.32 Microscope picture of pattered APSM film by Image reversal process........65

List of tables

Table 0.1 *APSM* film requirements:....................2
Table 1.1. Intel processors increase speed with more transistors inside....................4
Table 3.1 Basic deposition parameter setup....................30
Table 3.2 Ellipsometer film analysis process....................34
Table 3.3 Features of AZ5214E photoresists....................38
Table 3.4. Lift-off procedures....................45
Table 4.1 EMA model prediction for $Al\text{-}NbO_x$ *APSM* film....................46
Table 4.2 *Al-NbOx* fabrication parameter and characteristics....................51
Table 4.3 EMA model prediction for $Al\text{-}TaO_x$ *APSM* film....................52
Table 4.4 comparison of Al_2O_3 and TaO_x deposition rate....................55
Table 4.5 $Al\text{-}TaO_x$ deposition parameter setup from calculation....................56
Table 4.6 *Al-TaOx* fabrication parameter and characteristics....................59
Table 4.7 EMA model prediction for $Al\text{-}CrO_x$ *APSM* film....................61
Table 4.8 EMA model prediction for $Al\text{-}MoO_x$ *APSM* film....................62
Table 7.1 Materials' optical properties from RIT lithography group....................70

Acknowledgements

I wish to express my sincere acknowledgement to the following people for their generous support and great contribution to my thesis work: my advisor Dr. Bruce W Smith, Anatoli Bourov, Yongfa Fan, Professor Carl Hirshman. I also would like to extend my gratitude and appreciation to the Microelectronics Engineering Fabrication Laboratory of Rochester Institute of Technology and Corning Tropel for use of equipments and facilities.

Abstract

The Semiconductor Industry Association Roadmap 2003 has put 157 nm optical lithography as the next generation lithography wavelength for the node of 70 nm integrated circuits and below. The small departure from 193 nm puts more challenge on imaging tools and processes. One of the crucial areas is the exploration of thin film optical materials for mask coatings at vacuum ultraviolet (*VUV*) wavelength. Attenuated Phase Shift Mask (*APSM*) is one of the optical enhancement technologies pushing critical dimension of lithography to diffraction limits. As no existing single material satisfies those demanding requirements of *APSM*, non-stoichiometric composite materials will be explored to keep optical lithography from demise. In this case, the individual dielectric response of those constituents must be combined in an effective model to reproduce composite film dielectric response. The relationships between thin film microstructure and optical properties are extremely useful for the development and characterization of thin films. Effective Media Approximation (EMA) theory will bridge thin film composition and/or microstructure to optical properties.

APSM can improve both resolution and depth of focus with complexity in fabrication. It has become an attractive candidate to replace those of multilevel mask processes such as aligning, rim, or sub-resolution schemes. The *APSM* should have transmission between 4% and 15% with a π phase shift [1]. Also the thin film must be feasible to pattern. This thesis worked on several potential Al_2O_3 hosted composite materials. By carefully combining the absorbing and non-absorbing components based on the database of RIT lithography research group for optical properties of various materials, the optical

properties of the composite thin film can be tailored to achieve the desired requirements by adjusting the deposition conditions, which include reactive gas partial pressure, power and time. Four promising Al_2O_3 hosted composite materials were proposed and two of them were fabricated and tested with satisfactory results.

An image reversal lift-off process was adapted and modified for patterning of the *APSM* film. The lift-off process was able to pattern the *APSM* film with 2 microns critical dimension. Al_2O_3 hosted oxide non-stoichiometric composite materials satisfy all the *APSM* film requirements and can be patterned by lift-off process with reasonable critical dimension.

Criteria	Target Range
Transmission at 157 nm	4-15%
Transmission at 193 nm	below 50%
Reflectance at 157nm	Below 15%
Phase Shift at 157 nm	180 degree
Critical dimension of patterned film	2 micons

Table 0.1 *APSM* film requirements.

1. Introduction

1.1 Background and technology trend

Semiconductors, sometimes referred to as computer chips or Integrated Circuits (ICs), contain numerous electrical pathways, which connect thousands or even millions of transistors. These circuits buildup connections and networks, which fictionalize various chips to work for us. The microchip is everywhere in our modern society.

Microchip has been getting smaller, smarter, denser and much cheaper, which are all driven by the advancement of the manufacturing methods of ICs. Microlithography is one of the most enabling technologies that make this possible. Microlithography is the technology used to image a pattern from a photomask onto a silicon wafer coated with a light sensitive material called photoresist. Radiation is passed through photomask, exposing photoresist on the wafer and creating the blueprint for the metal that will be deposited on it. Wafers are eventually cut, layered and packaged together, forming Integrated Circuits.

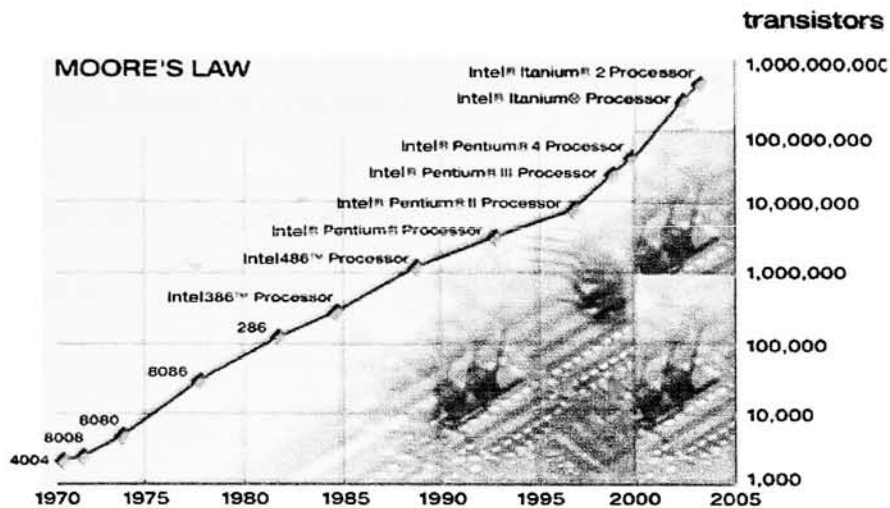

Figure 1.1 Moore's law and the future of lithography. In present incarnation of Moore's law, the storage density of memory chips doubles every 18 months [4].

	Year of Introduction	Transistors
4004	1971	2,250
8008	1972	2,500
8080	1974	5,000
8086	1978	29,000
286	1982	120,000
Intel386™ processor	1985	275,000
Intel486™ processor	1989	1,180,000
Intel® Pentium® processor	1993	3,100,000
Intel® Pentium® II processor	1997	7,500,000
Intel® Pentium® III processor	1999	24,000,000
Intel® Pentium® 4 processor	2000	42,000,000
Intel® Itanium® processor	2002	220,000,000
Intel® Itanium® 2 processor	2003	410,000,000

Table 1.1 Intel processors increase speed with more transistors inside.

More than a quarter century ago, when Intel was developing the first microprocessor, its company cofounder Gordon Moore predicted that the number

of transistors on a microprocessor would double approximately every 18 months. To date, Moore's law has proven remarkably right.

Some people have been predicting the demise of Moore's law while some others continually proved them wrong for years, no matter which side is right, it's for sure that we must keep pushing our ICs to be faster, denser and even cheaper than ever before.

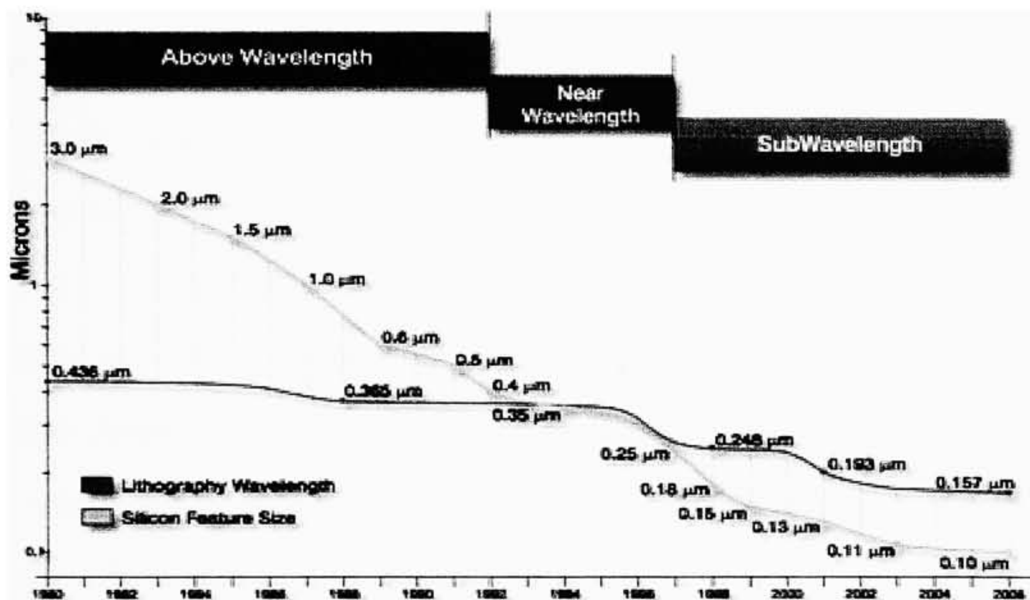

Figure 1.2. Microlithography goes to sub-wavelength [23].

Microlithography is the most important step in semiconductor fabrication process. Advances in microlithography have been the key for achieving the constant scaling down in line width of Integrated Circuits, imperative for speed increase and lowering power consumption. Optical lithography has been struggling for improvements because the critical challenges from every aspects like photomask materials, radiation source, photoresist, as we push to next generation microprocessors. Excimer lasers with a wavelength of 248 nm or even

193 nm are routinely used to fabricate devices at dimensions of sub-wavelength, and recent developments in 157 nm lithography has suggested that optical lithography may be used even further. Combined with chemically amplified photoresists, routine adoption of anti-reflective coatings and resolution enhancement techniques (*RET*), we are able to keep using optical lithography to pattern even smaller features.

Generally, there are three techniques of *RET*. First, radiation wave direction is controlled by designing special illuminators (off-axis illumination, OAI) to combines angle and pitch information of mask features to enhance certain spatial frequencies in the image. Second, wavefront amplitude is controlled by changing aperture sizes and shapes (optical process correction, OPC), to improve overall fidelity and reduce linewidth variation according to appropriate adjustments of certain portions of features on photomask layout. Lastly, local wavefront-phase is controlled by changing materials properties or etching structures into the surface of the mask (phase-shift masks, PSM).

The smallest printable feature is called critical dimension or resolution. Generally, the smaller the critical dimension of a device, the faster the speed of the device. Also, shrinking the linewidth of a device allows more devices to be put on each wafer unit area, leading to increased productivity and profit. A general form of optical lithography resolution according to Rayleigh's criterion is:

$$R = k_1 \frac{\lambda}{NA}$$

(1)

Where R is resolution (resolvable image), k_1 is a process-dependent factor that incorporates everything in a lithography process that is not wavelength (λ) or numerical aperture (NA), which is determined by the size and acceptance angle of the lens.

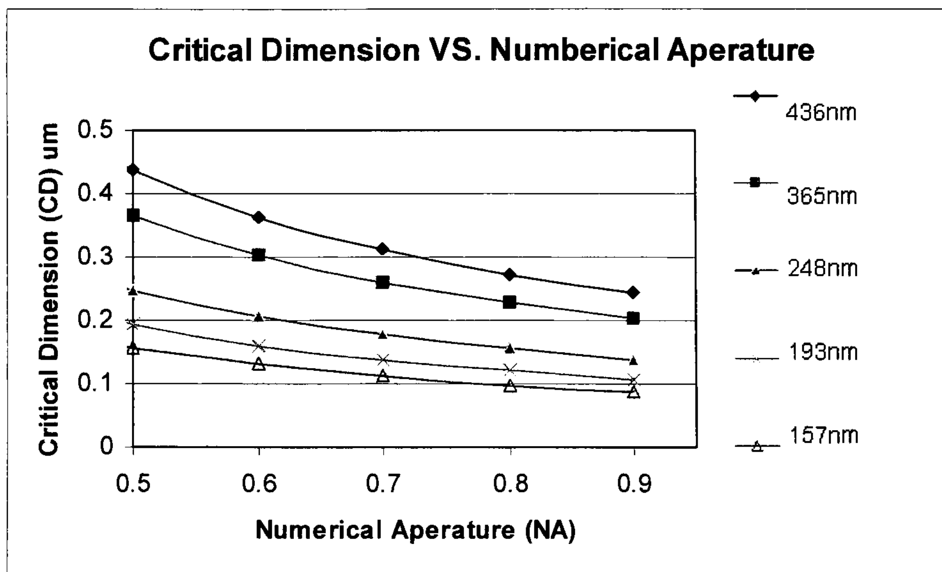

Figure 1.3. Critical Dimension (CD) vs. Numerical Aperture (NA) for different wavelengths.

We can see from Figure 1.3 the critical dimension decreases proportionally as numerical aperture increases and wavelengths decreases. For the same numerical aperture value, the smaller the illumination wavelength, the smaller the critical dimension. Depth of focus (DOF) needs to be considered along with resolution criteria for optical lithography. Depth of focus is defined as the distance along the optical axis that produces an image of some suitable quality [1].

$$DOF = k_2 \frac{\lambda}{NA^2} \quad (2)$$

Where k_2 is also a process-dependent factor. For a resist material of reasonably high contrast, k_2 is 0.5. DOF decreases linearly with wavelength and as the square of numerical aperture. So, we can see in order to get smaller resolution while keeping the same level of depth of focus, it is more desirable to lower wavelength than to increase numerical aperture.

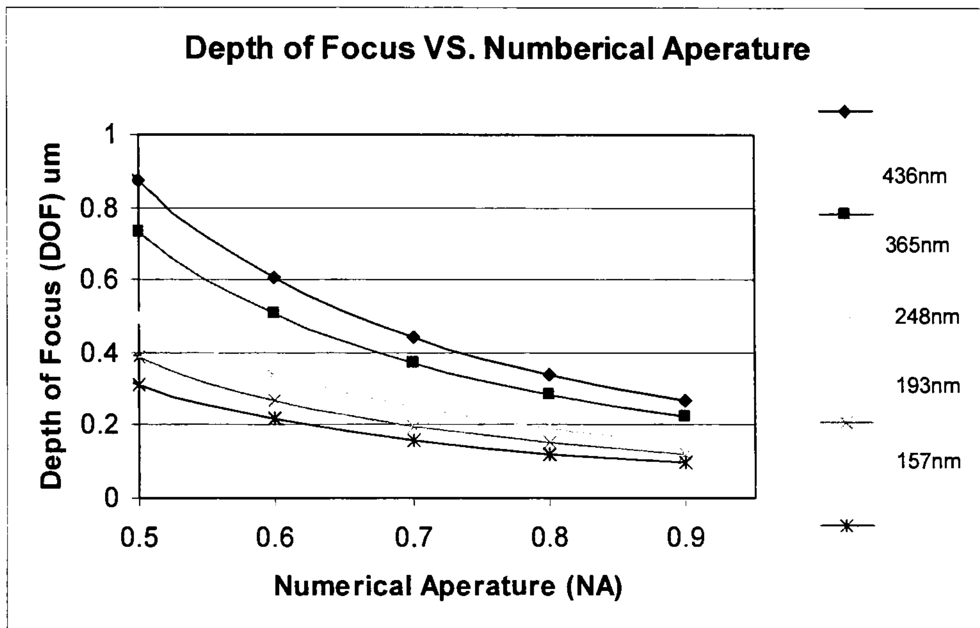

Figure 1.4. Depth of focus (DOF) vs. Numerical Aperture (NA) for different wavelengths

It can be see from Figure 1.4., depth of focus decreases as we go to shorter wavelength or/and larger numerical aperture, but wavelength does less to decrease depth of focus than numerical aperture does, this is because depth of focus is inversely proportional to the square of numerical aperture while proportional to wavelength.

An optical lithographic projection system is designed to transfer image correctly and accurately. The mask is designed to represent the ideal pattern that the circuit designer intends to put on the surface of the wafer. Any lack of fidelity in the image transfer caused by the mask will lead to an error in the printed circuits. To deal with smaller images, tighter process latitude tolerances, and greater data volumes of modern semiconductor manufacturing, masks need to be designed to minimize undesirable effects of optical diffraction. Also new materials and structures are required for the shorter wavelengths lithography. The mask industry has resorted to sophisticated *APSM* in order to extend optical lithography.

The concept of increasing resolution of lithographic image by modifying the optical phase of the mask transmission was proposed by Levenson in 1982 [2]. Several distinct types of phase masks have been invented. They all share the common feature that some non-transparent areas of the mask are given a 180° shift in optical phase relative to nearby transparent areas. The interaction between the aerial images of two features with a relative phase difference of 180° generates an interference node or dark band between the two features.

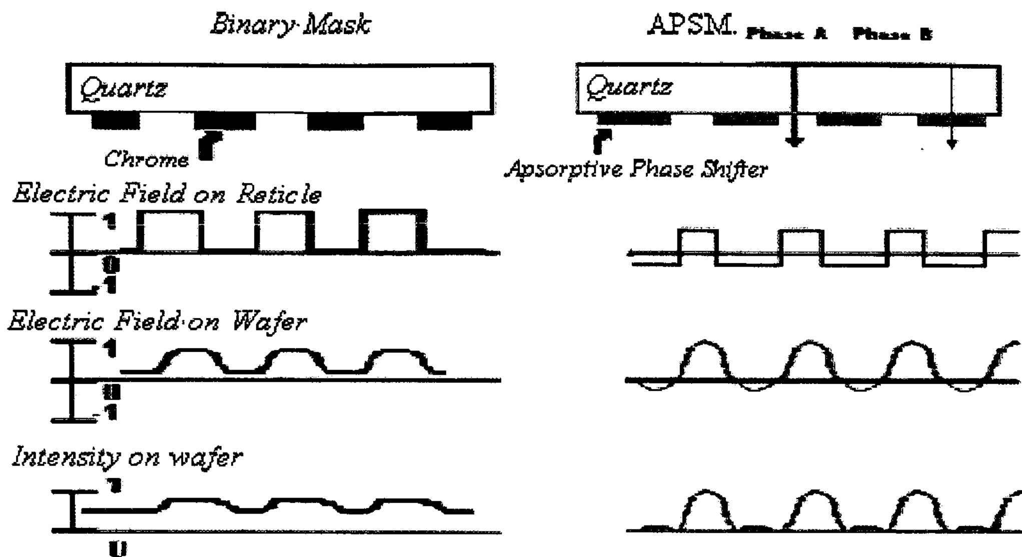

Figure 1.5. Comparison between Binary Mask and *APSM.*

APSM replaces the dark (less than 0.1% transmission) chrome with absorptive phase shifter, which can let 5-10% transmission pass through this area to get sharper image at the edge between dark and transparent areas on mask while those transmitted radiation through absorptive phase shifter is not strong enough to exceed the threshold value of current high-contrast resist to exposure the resist or degrade the desired image.

We can see this from Figure 1.5, for the conventional binary mask, the mask function as a filter, the opaque area intent to get zero radiation while the open area intent to get 100% transmission. Due to diffraction of light, the intensity under the opaque area is not zero, which will degrade image. For *APSM*, the opaque area is replaced by partially transmitting areas, which changes the phase of light with 180° relative to the clear regions. The total opposite phase of radiation along opaque and open areas will cause destructive interference.

Owing to destructive optical interference at the edges of circuit features, a phase-shifting mask (*PSM*) improves depth of focus and resolution. Because attenuated phase-shifting mask (*APSM*) can overcome phase conflict problems for arbitrary mask patterns and can be more easily fabricated than the other types of *PSM*, it becomes the most promising choice among *PSM*s. *APSM* uses a partially transmitting 180° phase-shifting film to replace the chromium absorbing layer on the mask. Interference between light from the transparent regions of the mask and phase-shifted light passing through the partially transmitting absorber gives a steeper slope of the aerial image of feature edges. Usually, transmission of the phase-shifting absorber ranges from 5 to 10% [21]. The partially transmitting absorber allows a few of undesirable radiation to fall on the photoresist, but the amount of those radiation is not enough to expose the photoresist.

The common metric used for measuring contrast is the image log slope, which is the slope of the aerial image formed at the interface of the clear and the dark regions. The improvement in the image log slope by using an *APSM* as compared to a conventional mask is illustrated in Figure 1.5.

From Figure 1.6, we can see how 0t, 1st, 2nd diffraction orders are influenced when an *APSM* is employed comparing with binary mask. The 1st and 2nd order diffractions of radiation are the most critical part to give the information to form the latent image in the photoresist [1]. These plots describe comparison between *APSM* and binary by changing transmission of *APSM* under different feature duty ratios. As we can see, *APSM* can decrease 0th amplitude and increase

amplitude for 1st and 2nd order of diffraction light especially around duty ratio of 1:1 (space to line). The advantage of *APSM* compare with binary mask can be seen by tailoring the transmission of *APSM* and determining a suitable solution for every specific duty ratio feature to get the most optimized latent image.

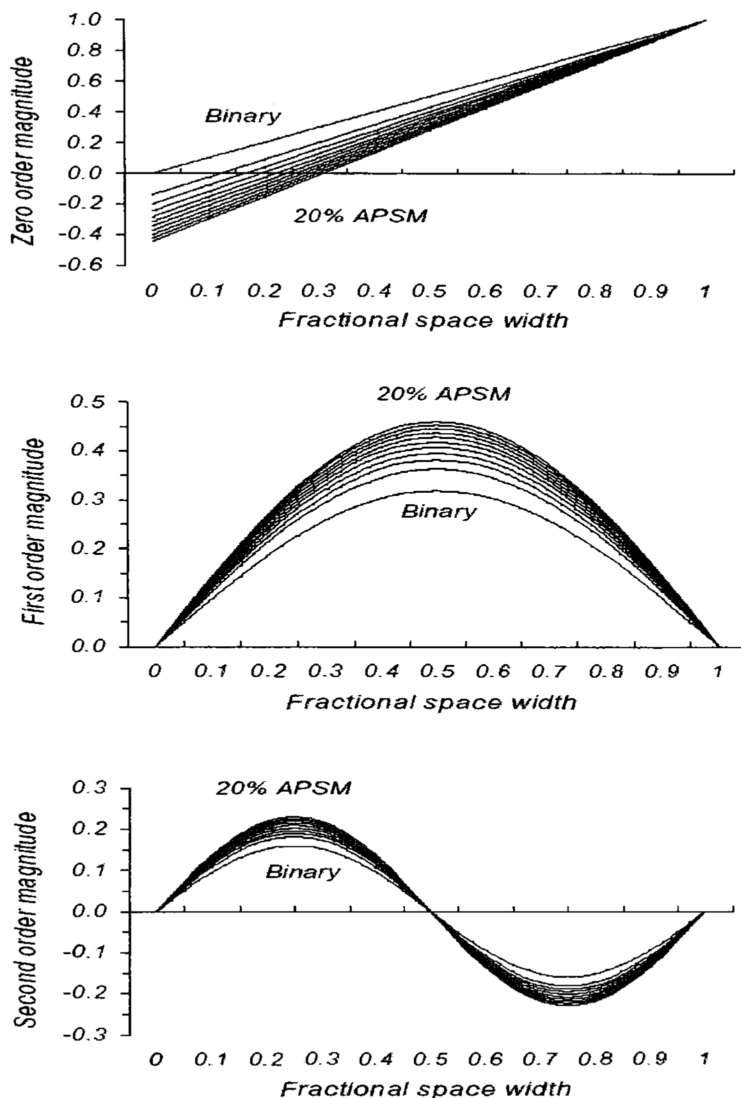

Figure 1.6. The 0th, 1st and 2nd diffraction order values for *APSM* transmission between 0% (binary mask) and 20% with 2% increments. Fractional space width value is the portion of the pitch value that consists of a space. Where 0.5 means 1:1 space/line ratio. As *APSM* transmission increases, the value of 0th order decreases while 1st and 2nd orders increase. [3].

2. Theory

2.1 Parameters of *APSM*

From basic optical theory, phase shift of incident radiation passing a transparent material is dependent on a films thickness (t), real refractive index of the material (n), and the wavelength of radiation (λ).

$$\phi = \frac{2\pi}{\lambda}(n-1)t \tag{3}$$

where ϕ is the phase shift value, real refractive index of air is 1.

Or the thickness of materials (t) giving exact 180° phase-shift can be expressed like this:

$$t = \frac{\lambda}{2(n-1)} \tag{4}$$

According to Beer's law of transmission, absorption (α) of light in any material is mainly affected by the extinction coefficient (k) in the formula (5) and the relationship between α and transmission (T) is from formula (6):

$$\alpha = \frac{4\pi k}{\lambda} \tag{5}$$

$$T = e^{-\alpha t} \tag{6}$$

The reflectivity of mask film is also very important. It will cause stray light or flare in the optical system. And high level of reflection will severely degrade image quality. Single surface reflectance (R) of any material with normal

incidence angle s expressed as:

$$R = \frac{[(n-1)^2 + k^2]}{[(n+1)^2 + k^2]} \tag{7}$$

So the total phase change of light through *APSM* compare with light through open areas is expressed as formula (9) when the contributions of interface are considered.

$$\Delta\phi = \Delta\phi_{(air-apsm)} + \Delta\phi_{(apsm-sub)} - \Delta\phi_{(sub-air)} \tag{8}$$

These additional interface phase shift terms are non-negligible as k increases, so relative lower k value materials are preferred.

Mask reflectivity should be lower than 15% as a rule of thumb [20]. Excluding the light reflectance off the top and bottom interfaces, the transmitted radiation through phase shifter is

$$T = \left[1 - \left|\frac{n - n_{air}}{n + n_{air}}\right|^2\right] \cdot \left[1 - \left|\frac{n - n_{sub}}{n + n_{sub}}\right|^2\right] \cdot e^{-\frac{4\pi k}{\lambda}t} \tag{9}$$

A deviation within 5° is acceptable for an *APSM* thin film [21]. Any deviation from 180° will reduce the image log slope. Even the image quality will be worse for *APSM* than binary mask if the phase error is too big. So, the *APSM* thin film should be designed, fabricated correctly and accurately to ensure the matching composition and thickness to give satisfactory phase shift.

2.2 Materials Screening for APSM

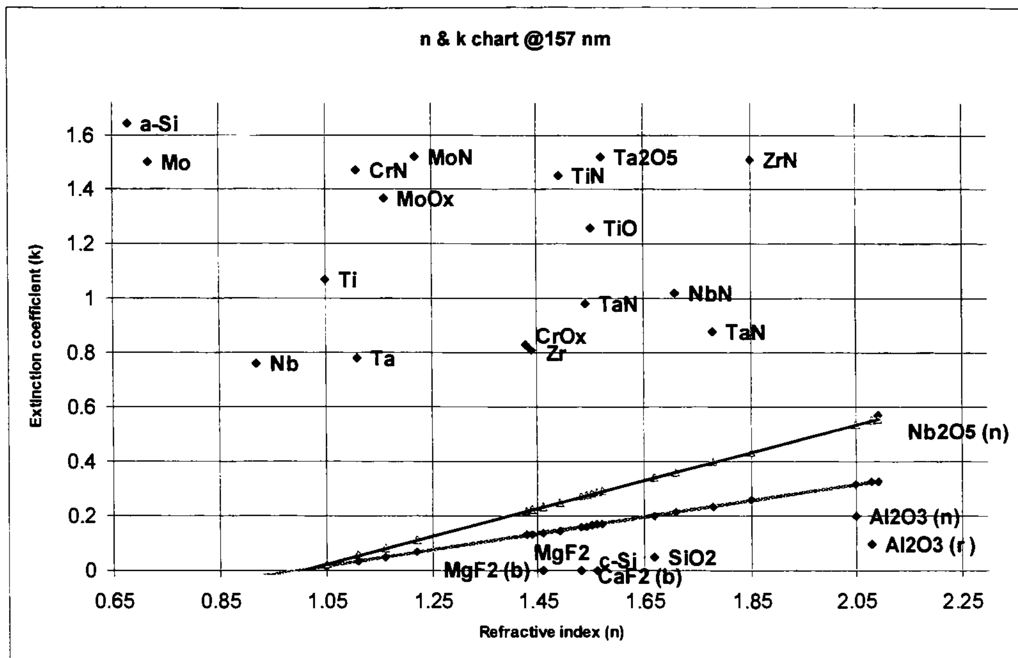

Figure 2.1.Diagram of materials refractive index and extinction coefficient diagram at 157 nm [22].

The Refractive index and extinction coefficient diagram is constructed based on the database of material evaluation for *APSM* [22]. For 157nm, where a narrow wedge has been identified for materials that can produce a 180° phase shift with transmission between 4% and 15% at appropriate thickness. This wedge has been created based on first order phase calculation, neglecting interface effects as described in above Figure 2.1.

As suggested from the data, it is not likely that elemental thin films or compounds exist which satisfy *APSM* requirements at 157 nm. Inspection of the optical properties of these materials does indicate, however, that non-stoichiometric compounds or composites of these materials may offer solutions.

A wider range of material properties are possible by relaxing stoichiometric requirements. By controlling the ratios of material components during deposition, optical behavior can be modified. Furthermore, by co-sputtering or by forming graded films, some candidates are possible.

Through use of the data in Fig. 2.1, several material combinations have potential for application as *APSM* at 157 nm can be proposed. The interest in this thesis is to research several groups of thin films hosted by Al_2O_3 combined with other oxide materials as *APSM* for 157 nm.

2.3 Consideration of *APSM* at 157nm

The basic requirement for *APSM* film is to offer a 180° phase shift of transmitting 157nm radiation with transmission around 10%. At the same time, reflectivity should be as low as possible because any unwanted stray of light will deteriorate image quality and resolution. And most of the reflectance is from the *APSM* film surface. From Figure 2.1, we can conclude that in order to get small reflectance from the APSM, we need a material with relative lower n and k.

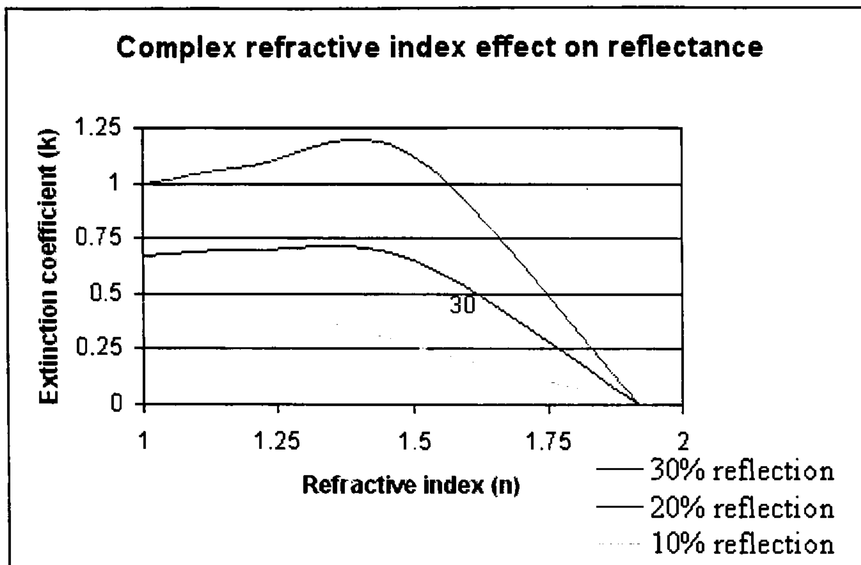

Figure 2.2 n and k effect on reflectance. From top to bottom is a set of complex index chart of three series of materials which can offer 30%, 20% and 10% respectively of interface reflectance between film and air when radiation reflect upon the film. Calculation is based on formula (7).

Also the transmission of alignment radiation, which is needed to position this reticle correctly in the stepper needs to be lower than 40% [21]. Normally the inspection or alignment wavelength is longer than the exposure wavelength, so probably 193 or 248 nm is used for 157nm stepper. All these above requirements place a very narrow range for us to select our *APSM* materials, which is almost impossible to find in any naturally occurring elemental or composite materials. So we need to move our sight from stoichiometric materials to non-stoichiometric materials.

2.4 Modeling

In order to characterize the film accurately, a realistic model of complex refractive index of for the thin film materials is needed. It must be able to accommodate for the surface and interfacial roughness, thickness non-

uniformity, grain boundaries, voids and other disordered regions. Besides the homogeneous materials, it is usually necessary to determine the optical properties of heterogeneous or composite systems and superlattice structures that are more accurately described as mixtures of separate regions of two or more materials [5]. Generally, heterogeneous materials consist of microscopic regions that are orders of magnitude smaller than the wavelength of light, yet large enough to retain their own dielectric properties. So, we need to take into consideration those individual components of the composite materials and their relationship for our model. Grain boundaries, voids and other structural inhomogeneities affect the *uv/vuv* optical properties of materials. The dielectric response of an individual homogeneous region depends on its composition and presence of long range order (such as grain size). Optical constants of materials define how light interacts with a material.The real part or index of refraction, n, defines the phase velocity of light in material:

$$n=c/v \tag{10}$$

Where v is the speed of light in the material and c is the speed of light in vacuum.The imaginary part or extinction coefficient, k, is directly related to the absorption of material.It is related to the absorption coefficient α, λ is the wavelength of light. Optical constants vary with wavelength and temperature. To predict and interpret thin film optical behavior, appropriate models based on constituent material properties and certain assumptions are required.

For a given species (atom, molecules, etc.), electric dipole moment E'

$$\mu = \alpha E' \tag{11}$$

$P = N\alpha$ $E' = E$ for gases but not solids.The electric displacement vector D is related to E by $D = \varepsilon E = E + 4\pi p$, where ε is the dielectric constant or function, which may be a scalar or tensor. So, we can say

$$\varepsilon = 1 + 4\pi P \tag{12}$$

The local electric field usually differs from the applied electric field (from the light source) because of the field produced by the local polarization. For isotropic media, these fields are related by $E' = E + 4\pi P/3$, the last term being the Lorenz field produced by local dipoles.

The microscopic polarizability α is related to the dielectric constant by the Lorentz-Lorenz formula

$$\alpha = \frac{3}{4\pi N}\left(\frac{\varepsilon - 1}{\varepsilon + 2}\right) \tag{13}$$

Optical constants (n, k) are routinely related to electrical properties (ε', ε'') of materials by neglecting material structure and considering macroscopic material quantities only. The real and imaginary parts of the dielectric constant and index of refraction are related by

$$\varepsilon' = n^2 - k^2 \tag{14}$$

$$\varepsilon'' = 2nk \tag{15}$$

The inverse relations can be obtained from

$$k^2 = \frac{\sqrt{\varepsilon'^2 + \varepsilon''^2} - \varepsilon'}{2} \qquad n^2 = \frac{\sqrt{\varepsilon'^2 + \varepsilon''^2} + \varepsilon'}{2}$$

(16), (17)

In order to account for material structure, Drude analysis of optical and electrical constants describes free electron or metallic behavior of materials quite well in the visible and *IR* region. To account for optical properties at shorter wavelengths, Bound Electron Theory needs to be utilized. For dielectric materials, no intraband transitions exist because of filled valence bands. Interband transitions are also limited in *IR* and visible regions because of large band gap energies. Bound electron theory alone is sufficient to describe classical dielectric material behavior. Characterization of metallic and non-insulating materials in *UV* and visible regions requires use of both free electron and bound electron theory. By assuming a given number of free electrons and a given number of harmonic oscillators, optical properties of materials over a wide wavelength range can be described. Models described here provide a quantitative description of the macroscopic dielectric function of a heterogeneous material in terms of its composition and microstructure [4]. Since precise microstructure is unavailable and would be unpractical for use even if absolute limits on the dielectric function are obtained. Assumption of macroscopic homogeneity has been made, which in practice means that any inhomogeneity considered has a structure size smaller than 0.1λ. Optical constants (n, k) are routinely related to electrical properties (ε, ε'') of materials by neglecting material structure and

considering macroscopic material quantities only. In order to account for material structure, ***Drude analysis*** of optical and electrical constants describes free electron or metallic behavior of materials quite well in the ***visible*** and ***IR*** region [4].

2.5 Modeling of thin film optical properties

Grain boundaries, voids and other structural inhomogeneities will affect *UV/VUV* optical properties of materials. The dielectric response of an individual homogeneous region depends on its composition and presence of long range order (such as grain size). Screening charge develops on grain boundaries, causing difference between local and applied field. The effectiveness of this screening effect depends on the shape and size of the grains. Since the dielectric function is defined as the dipole moment per unit volume, the density of the film should also affect the dielectric response. Models should be able to provide a quantitative description of the macroscopic dielectric function of a heterogeneous material in terms of its composition and microstructure. In order to account for all the above requirements, some assumption are necessary, the thin film material is macroscopic homogeneous, which means any inhomogeneity should has a structure size smaller than 0.1 λ.

If a phase is homogeneous, its dielectric function can be obtained from literature. Dielectrics are often simulated by using Lorentz oscillator model.

Microscopically inhomogeneous phases are often modeled using the effective medium approximation (EMA) (Aspnes, 1982 and Chang, 1989" Jellison, 1993).

When the dielectric functions of composite constituent materials (a and b) are available, the dielectric constant of the composite material can be expressed as the Lorenz-Lorenz effective media approximation below. Where f_a is the volume faction of one material a.

$$\frac{\varepsilon - 1}{\varepsilon + 2} = f_a \frac{\varepsilon_a - 1}{\varepsilon_a + 2} + f_b \frac{\varepsilon_b - 1}{\varepsilon_b + 2} \tag{18}$$

In the most widely used EMA, the effective dielectric constant ε is given by the Bruggerman expression. This assumes two randomly mixed phases with dielectric constants $\varepsilon_a$and ε_b with fractions f_a and f_b respectively. The dielectric constant of the composite material can be expressed by the Lorentz-Lorenz effective approximation and also can be extended for more than two phases. The Maxwell-Garnet EMA is an alternative approach that assumes layered phases.

A general expression of the dielectric function can be expressed as:

$$\varepsilon = \frac{\varepsilon_a \varepsilon_b + \bar{\varepsilon}(f_a \varepsilon_a + f_b \varepsilon_b)}{\bar{\varepsilon} + (f_a \varepsilon_b + f_b \varepsilon_a)} \qquad \bar{\varepsilon} = \frac{(1-q)\varepsilon_h}{q}$$

(19), (20)

ε_h is dielectric function of the host material (typically material with higher composition) and q is the depolarization factor (microstructure parameter). If q is 0, it means all the boundaries inside materials parallel to the field applied and q=1 means all the boundaries perpendicular to the field applied. When q between 0 and 1 represents practical situation. For example, q=1/3 means an atomistic level mixed material [7]. EMA is based on a solution of the Lorentz-Lorenz problem and provides the connection between the microstructure of a heterogeneous thin film and its macroscopic dielectric response ε, where f_a and f_b are the volume percentage of each constituent materials in the composite materials.

Optical properties of a composite thin film may be explained in terms of its anisotropic electrical properties on a scale larger than the molecule. Namely, the ordered arrangement of similar particles of optically isotropic material's size is large compare with the dimensions of molecules, but is less than the wavelength of light. Let's consider a simplified case of regular assembly of a laminate of thin layers of component separated by thin layers of components under the condition that the linear dimensions of the faces of the plates are large but the thickness t_1 and t_2 small compared to the wavelength.

The models have been expanded to include more than two constituents, which is useful especially for composite masking films. In general, if ε_1 and ε_2 are similar, then ε is determined almost entirely by the composition and is

essentially independent of microstructure. If ε_1 and ε_2 are substantially different, then microstructure is the dominant variable [20].

2.6 Photoresist patterning: lift-off process

Generally, positive photoresist is a three-component mixture of an alkaline soluble novolac resin, a photosensitive dissolution inhibitor, often called Photo Active Compound (PAC) and a carrier solvent. PAC serves to retard the dissolution rate of the novolac resin in alkaline solutions. When exposed to proper wavelength and sufficient energy, the PAC will undergo photochemical decomposition, which renders the polymer soluble in an alkaline developer. The PAC is a diazoketone, which upon exposure to ultraviolet radiation generates a highly reactive intermediate ketene and liberates nitrogen. The ketene will react with available water to form an indene carboxylic acid, which is now soluble in the basic developer. This is called positive photoresist because the clear areas of the mask remain as clear areas in the photoresist. The molecular weight and exact percentage of solids is tightly controlled to assure exceptional film thickness uniformity [15].

Image reversal of positive resist is capable of improving resolution, sidewall angles, and process latitude. Based on novolac resists, new chemistry with 'blocked' reactive agents has been developed. The reactive agent can be thermally liberated from the resin, or be photochemically generated. It will react with indene carboxylic acid groups in the exposed area to render this area

insoluble after being generated. The flood exposure converts the remaining photoactive compound in the resist layer after postbake. Finally, development gives negative image of the mask. The crosslinking between reactive agent and indene carboxylic acids groups during processing improves the photoresist contrast because both of them are photogenerated. The crosslinking is a second order reaction based on two photogenerated species, the concentration gradients in the film are sharper than a single PAC system, which follows first order kinetics [19]. This feature will improve resolution, contrast and process latitude. Another great benefit of image reversal is good thermal stability comes with the formation of crosslinked negative images, which is very helpful for PVD deposited *APSM*. Our film is fabricated in a relative hotter process (>100C^{o}), so the thermal stability of the photoresist is a major concern and it's related to the pattern of the film directly.

The kinetics of the image reversal is dependent on the initial exposure energy, temperature and duration of the post exposure bake and various ambient conditions, which all can be explained by the crosslinking mechanism. Upon exposure, the photoactive compound generates an acid. Because of the unique structure of the photoactive compound used in the AZ5214E, this acid is much stronger than is typically generated in most commercially available photoresists. Following the relatively high temperature of the post exposure bake, this acid diffuses through the resin system of the film and cause acid catalyzed crosslinking. Sub-micron geometries can be printed by limiting the diffusion of

the acid through control of the quantity of the acid photogenerated and the temperature and duration of the post exposure bake.

AZ5214E is intended for lift-off techniques, which calls for a negative wall profile. Although they are positive photoresists comprised of a novolac resin and naphthoquinone diazide as photoactive compound. They are capable of image reversal resulting in a negative pattern of the mask. In fact AZ5214E is almost exclusively used in the IR-mode. Photosensitivity of a resist has its origin on photoactive compound (PAC), which is consumed during exposure. Once fully exposed, the resist volume will no longer contain unreacted PAC. In AZ5214E, catalyst is formed simultaneously in the volume of exposed resist that promotes polymer cross-linking during any heat treatment later. The crosslinking agent becomes active at temperatures above 110 °C [13]. They are only active in exposed areas while the unexposed areas still behave like a normal unexposed positive photoresist. Polymer cross-linking will make the exposed resist volume more resistant against developer attack. After baking the exposed sample, the image reversal process is completed by exposing the whole sample area. The purpose of a flood exposure is to turn those resist areas that were originally shielded by a mask soluble to developer, which means they still function as positive resist. Cross-linked areas contain little or no PAC, so flood exposure will not reduce solubility considerably there. After development, the pattern of resist is a negative image of the original in mask.

3. Experimental

3.1 Thin Film Deposition

Thin film deposition was used to apply thin coatings of *APSM* films. Thin films generally have thickness less than a few microns. They can be as thin as a few hundred angstroms. Thin film deposition techniques require a vacuum environment.

Physical Vapor Deposition is a technology in which the material is released from the source at much lower temperature than evaporation. The substrate is placed in a vacuum chamber with the source material, named a target, and an inert gas (such as argon) is introduced at low pressure. Radio Frequency power source is used to ignite plasma, causing the gas to become ionized. With RF-sputtering, the sputtering plasma is generated by an oscillating power source. It can be used to deposit both conductors and insulators, hence compound materials. During sputtering, ions are accelerated towards the surface of the target, causing atoms of the source material to break off from the target in vapor form and condense on all surfaces on their paths. A schematic diagram of a typical RF sputtering system is shown in the Figure 3.1.

Thin film process by sputter deposition has many advantages. The low-temperature processing is a unique feature that distinguishes sputtering from evaporation. The temperature is low enough not to degrade the photoresist I used for the definition of our *APSM* films during next image reversal lift-off process. The sputtering deposition is implemented in a plasma environment rich in charged particles. Therefore, electric and magnetic fields can be employed to direct the flow of atoms and molecules in the system.

Through low energy ion irradiation during film growth, the micro structural control of the film might be realized. At the time, many species in the plasma are more chemically reactive because they are at their excited states. The deposition of a compound film is therefore possible by reactive sputtering instead of sputtering a compound, which requires a harsh high voltage condition or a CVD process at high temperatures. The sputter rate of aluminum and other candidate materials will be studied as a function of power. In addition, the basics of reactively sputtered deposition thin films will be introduced. Specifically, the effect of the composition of the sputter gases on deposition rates, and optical properties will be studied.

A simplified depositing system is illustrated in Fig.3.1. Inside the working chamber, there is a pair of parallel metal electrodes. The cathode is the target to be deposited, and the anode is the substrate. The anode is usually grounded while the cathode is connected to the negative terminal of a RF power supply with a typical voltage of several kilovolts. A working gas, typically argon is introduced to the chamber to serve as the plasma media after the chamber is evacuated. The pressure of the working gas may range from a few to a hundred mil-torr. An appropriate voltage and power are necessary to maintain a visible glow discharge between the electrodes. A very small portion of the working gas, e.g. argon is ionized in the glow discharge:

$$e^- + Ar \rightarrow 2e^- + Ar^+ \quad (21)$$

The electric field drives the positive ions toward the cathode. Given sufficient energy, they can physically sputter target atoms through momentum transfer when striking on the target. If surviving collisions with molecular particles and electrons in the media, the sputtered target atoms may eventually deposit on the substrate to result in a thin film.

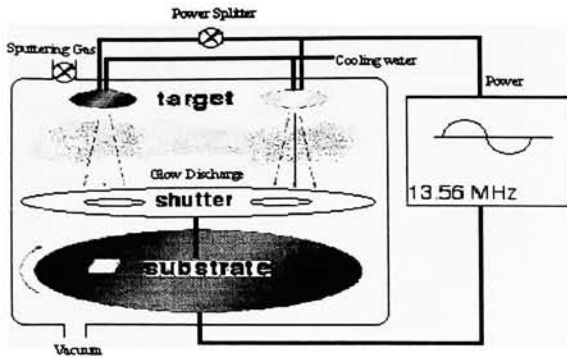

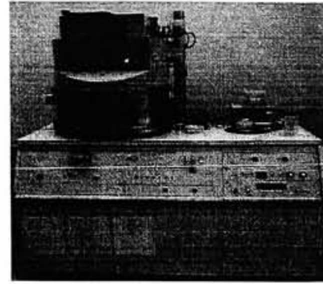

Figure 3.1. Illustrations of PE2400A RF sputter system configuration and outside view.

Our vacuum system uses one mechanic pump to pump from atmospheric pressure to 10^{-3} Torr, and another cryo-pump to achieve high vacuum from 10^{-3} to 10^{-7} Torr. The cryo-pump only work under vacuum offered by the mechanical pump, both of the pumps must be on when the PVD system is working.

In the presence of a reactive gas during the process of sputtering, thin films of compounds are deposited on the substrates. The most frequently employed gases are oxygen to form oxides, nitrogen to form nitrides. Depending on the depositing conditions, the resultant film could be a solid alloy solution of the target metal doped with the reactive element, a compound, or some mixture of the two. Exemplified in Figure 3.2 is the reactive sputtering deposition of *TaN* film at DC voltages of 3000 to 5000 voltages and pressure of 30 *mTorr*. As illustrated, the composition of the film is a function of N_2 partial pressure.

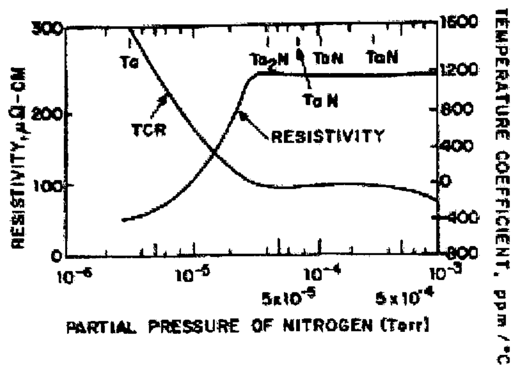

Figure 3 2. The film composition as a function of N_2 in DC reactive sputtering of Ta [9].
By controlling the partial pressure and voltage, the composition of the deposited film can be adjusted.

Reactive sputtering has advantages over directly sputtering compound targets. Note that pure metallic targets are cheaper and easier to buy than compounds targets. Also, they allow to make thin films with diffe ent compound or elementary thin film just by controlling process conditions. Our *APSM* thin films were fabricated by Perkin Elmer 2400A PVD system, which is a RF magnetron-enhanced sputtering system. The films are reactive sputtered and some fabrication parameters are listed in Table 3.1.

Power	500-1500 w
Base Pressure	2E-6 Torr
Deposition Pressure	8-12mil Torr
Pre-sputter Time	15 min
Deposition Time	50-90 min
Rotation Speed	2 rpm
Reflected Power	0 micro Ampere
Reactive gases	Argon, oxygen, nitrogen
Target size	8 inches
Substrate	High quality quartz and Si wafer

Table 3.1 Basic deposition parameter setup.

Prior to deposition, all substrates are cleaned and dehydrated. Films are deposited without additional substrate heating. Plasma is ignited to warm up at least 15 minutes to eliminate any oxidized or reacted materials on the target so pure target material is exposed later to plasma bombardment to deposit purer films. After pre-sputtering, shield between plasma and targets are removed by shield rotation. Target is strike by plasma particles, so that the wanted materials are stroke off to substrate on the deposition table. During deposition, the substrate table is rotating at speed of 2 rpm, which gives more even deposited film. The target is heated when the high voltage is applied and also the plasma is hot, a water cooling system is hooked up to the backside of all the targets to get rid of the excess heat generated by the PVD process. By setting up the gas ratio between argon and reactive gas such like oxygen, the decisive parameter of the composition of deposited film is only the voltage applied to each target, which means we have easier control and less complexity during deposition process.

3.2 Determination of *n* and *k* of thin film

3.2.1 Ellipsometry:

Ellipsometry is a sensitive optical analysis technique for determining properties of surfaces and thin films. Polarization state of incident light will be changed when reflected from a surface. The change of the shape and orientation of the ellipse depend on the angle of incidence, the direction of the polarization of the incident light, and the reflection properties of the surface. We can measure the polarization of the reflected light with a quarter-wave plate followed by an analyzer; the orientations of the quarter-wave plate and the analyzer are varied until no light passes though the analyzer. From these

orientations and the direction of polarization of the incident light we can calculate the relative phase change, Δ, and the relative amplitude change, ψ, introduced by reflection from the surface. An ellipsometer measures the changes in the polarization state of light when it is reflected from a sample. If the sample undergoes a change, for example a thin film on the surface changes its thickness, then its reflection properties will also change. Measuring these changes in the reflection properties can allow us to deduce the actual change in the film's thickness and or other properties. The sensitivity of an ellipsometer allows the detection of a few Angstroms change of thin film thickness. The ellipsometer is used to measure ψ and Δ, and thus the film thickness and refractive index can be calculated. Since the equation contains complex quantities, its solution is usually done by a computer or programmed calculator. Because ellipsometry measures the ratio of two values, it can be highly accurate and very reproducible.

3.2.2 Ellipsometer measuring process

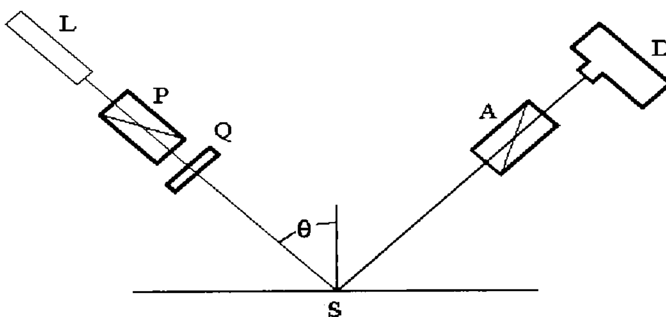

Figure 3.3. A schematic diagram of a nulling ellipsometer with the quarter-wave plate placed before the light is reflected from the sample. L: the light source; P: the polarizing prism; Q: the quarter-wave plate compensator; S: the sample under study; A: the analyzer prism; D: the light detector [10].

It shows a basic schematic diagram of a nulling ellipsometer with a quarter-wave plate positioned before reflection. L represents an unpolarized monochromatic light source that is collimated with a small beam divergence. A mercury lamp with a green filter and collimator serves this purpose. The mercury light is initially linearly polarized. When a polarized light source is used, the light is circularly polarized just after it emerges from a quarter-wave plate. The polarizer, P, follows the light source followed by the compensator, Q. The compensator is mounted in a holder so that its plane is perpendicular to the light beam and the angle measured from the plane of incidence to its fast axis, can be measured. The angle is measured the same as P. Following the sample is the analyzer. The analyzer angle, A, is again measured from the plane of incidence to the analyzer transmission axis by an observer looking into the beam. I used a J.A.Woollam WVASE Spectroscopic Ellipsometer, which has a spectroscopic range from 140 to 1400 nm. 157 nm is our interest of research. Also this ellipsometer use Variable Angle Spectroscopic Ellipsometry (VASE). It means it can change the incident angles of measurements during each set of measurement, which can offer more information about the film property and build more reliable and realistic model to for ellipsometric analysis.

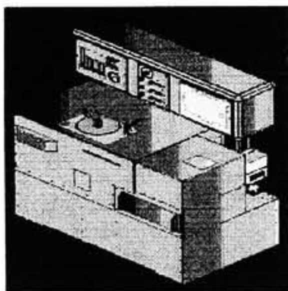

Figure 3.4. J.A.Woollam WVASE spectroscopic ellipsometer. This system has light range from 150 *nm* to 1800 *nm*, which is enough for our measurements.

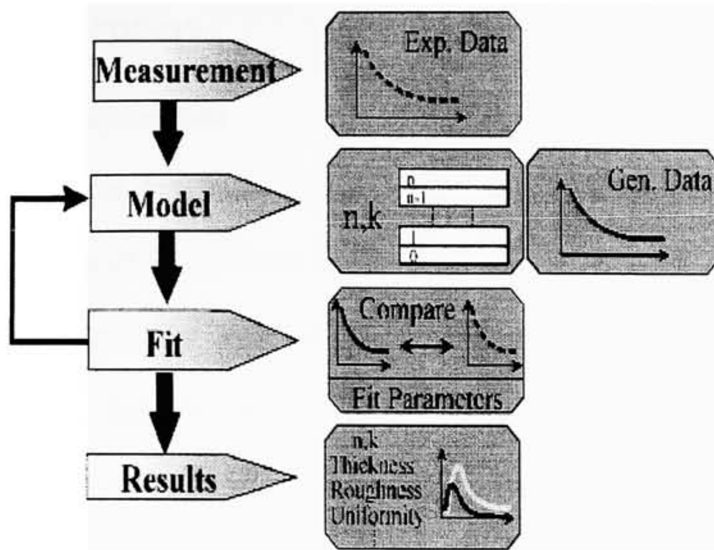

Figure 3.5. Data analysis flow-chart [11].

1	Acquired experimental data through measurement. Data was typically acquired versus wavelength and angle of incidence.
2	Built an optical model upon our film structure and process using as much information about the sample as possible. It is important to account for all layers in the sample structure.
3	Generated theoretical data from the optical model that corresponds to the experimental data based on the database.
4	Compared generated data to experimental data by fitting using WVASE software. In this process, those unknown parameters in the optical model, such as thin film thickness and/or optical constants, were varied to try and produce a "best fit" to the experimental data. Regression algorithms are used to vary unknown parameters and minimize the difference between the generated and experimental data.
5	Physical parameters of the sample such as film thickness, optical constants, composition, surface roughness, etc. were obtained once a good "fit" to the experimental data is achieved

Table 3.2 Ellipsometer film analysis process:

3.3 Lift-off process

3.3.1 Process consideration

The lift-off part was done at RIT micro-electronics engineering fabrication cleanroom, I conducted a series of experiments to verify the validity of image reversal as a technique to produce the repeatable and controllable photoresist profiles needed for a composite thin film "lift-off" process. One of the most basic mistakes one can commit during the preparation of an experiment of lithography is to rush a proven-to-be good recipe that originally developed by other testers. I modified Dr. Hirshman's lift-off recipe, which is designed to pattern pure evaporated metal film (above 2000 angstroms). For evaporation, the deposition process is more of line of sight process, which does not require negative profile of photoresist before they put down the film as our process because for physical vapor deposition process plasma permeate every space of the PVD chamber. Also we need to make sure the higher PVD working temperature does not "burn" or "reflow" the photoresist we used to lift-off the film.

"Lift-off" is a simple, easy method to pattern deposited films. A pattern is defined on a substrate using photoresist. A film is blanket-deposited all over the substrate, covering the photoresist and areas in which the photoresist has been cleared. During the actual lift-off, the photoresist under the film is removed with solvent, taking the film with it, and leaving only the film, which was deposited directly on the substrate. The motive for a lift-off process is the need to pattern metal lines on semiconductor substrates where the use of chemical or plasma etching is either undesirable or incompatible with the process or materials involved. Our APSM films are aluminum oxide hosted composite materials.

Etching these materials would require very harsh chemicals that would severely attack the mask substrate and decrease the process latitude. Lift-off is more desirable since the solvents used to remove the insulator in lift-off cause less damage to the underlying substrate than do the etch processes. Secondly, lift-off is applied when tight linewidth control is required. For 157nm lithography, tight control of APSM mask linewidth is essentially to the correction transfer of image. Error from variation of etch process will be eliminated since lift-off process depends only on the control of the photoresist.

Depending on the type of lift-off process used, patterns can be defined with extremely high fidelity and for very fine geometries. For example, it's the choice for patterning e-beam written metal lines. To achieve good lift-off, firstly, it's necessary to have a clear separation between the deposited *APSM* film on the resist layer and the *APSM* film on the open substrate areas directly, which means the deposited *APSM* film is not continuous at the edge of the resist profile, so we can actually "lift" the unwanted *APSM* film by removing the photoresist layer underneath it. So, the controlling of the resist edge profile is crucial, which means a negative slope is preferred or necessary.

Image reversal process can turn a positive slope into negative by reversing 'everything'. It was first adopted by IBM and since then numerous ways of image reversal methods have been tried [12]. The objective of the following experiments was to verify and modify a image reversal process for patterning my *APSM* film. The process must be capable of being used on a routine basis, in a repeatable and controllable manner. I inspected the resist profiles produced by the optimum process conditions and verified the

linewidth by SEM and spectrometer.

3.3.2 Image reversal process

The AZ5200 Series positive photoresist I used for lift-off were developed to operate at shorter wavelengths to take advantage of the inherently better resolution. These photoresists offer exceptionally straight sidewalls and wide process latitude to meet the growing demands of sub-micron lithography. It can image reverse to a negative tone using post-exposure bake (PEB), making it one of the most versatile photoresists available. The AZ5214E photoresists physical and chemical properties can be found from "AZ 5200 Positive Photoresists, Hoechst Celanese Corporation data sheet" [16].

After analysis of the image reversal process, the exposure dose and post-exposure bake temperature were found the most important parameters during the process, which are crucial to the negative side-wall of the resist profile. Also the hard bake should not be too high, otherwise it will reflow the resist and degrade the negative edge profile. The sputtering process of the *APSM* film is a high temperature process compare with the lithography process, which may degrade the resist by hardening or decomposing it. We should be able to monitor the sputter process to make sure the resist profile is not changed dramatically by PVD deposition. In addition, the PVD process is more conformal than evaporation process. All the above areas need to be checked to make sure we get the good lift-off results. Its broad spectral sensitivity in the negative tone allows a wide variety of exposure tools to be used, including g-line steppers and excimer lasers.

1	Near vertical profiles to give accurate pattern transfer.
2	Wide process latitude.
3	Excellent resolution in both metal-ion-free and inorganic developers.
4	High thermal stability (extended up to 250° C) to maintain profile quality during plasma etching, ion implant processes and thin film deposition.
5	Sub-micron resolution capability.

Table 3.3 Features of AZ5214E photoresists [16].

3.3.3 Processing and analysis

Based on our analysis and knowledge from experience and photoresist properties, plus recommendation from various literatures and laboratory colleagues, I organized and detailed the following processing procedures of AZ5214E lift-off process for the PVD fabricated Attenuated Phase Shift Mask composite thin films.

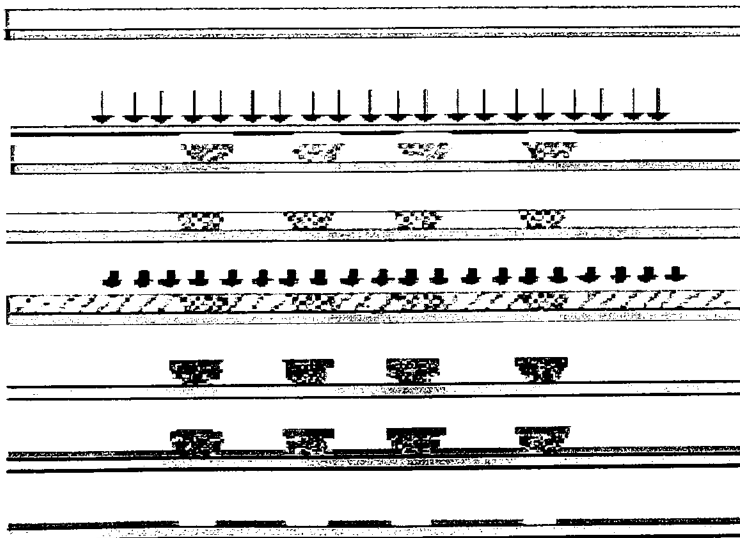

Figure 3.6 Image Reversal Lift-Off process flow chart

Substrate should be free of organic contamination or excessive physically absorbed moisture to eliminate the adhesion problems and improve the coating results [13]. Wafers should be baked for a period of time long enough to evaporate the excess water out and then the surface is treated by hexamethyl disilazane (HMDS), which is spin coated. The purpose of this step is to introduce an intermediate layer of HMDS molecules between the wafer surface atoms and the photoresist. HMDS surface layer is also able to seal the sample surface from moisture. The dehydration and priming process (is accomplished by the 4" SSI wafer track (program #4: 200° C for 5 minutes dehydration bake and 105° C for 45 seconds after HMDS application, details can be checked at Table 3.4). Substrates should be coated promptly after surface preparation. Take a spinner with a vacuum chuck to coat wafer with AZ214E.

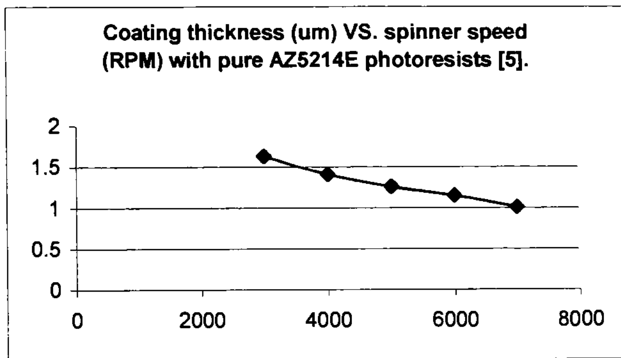

Figure 3.7 AZ5214E coating thickness (angstrom) VS. Spinner speed (rotation per minute)

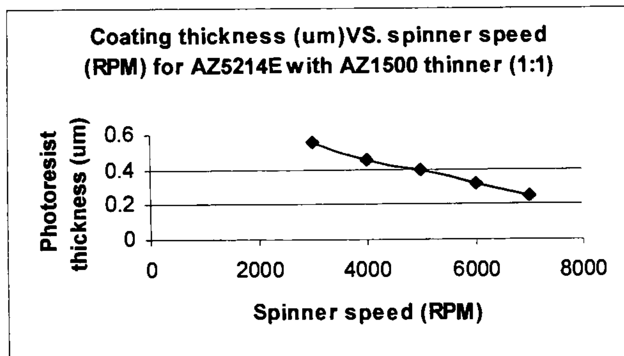

Figure 3.8 AZ5214E diluted with AZ1500 thinner (1:1) coating thickness (angstrom) VS. Spinner speed (rpm)

The *APSM* thin film thickness is about 800 angstroms. The photoresist thickness for the lift-off process should not be too thick or thin to function properly to lift-off. The best photoresist thickness is about 3-5 times of the deposited thin film thickness [18]. Spin speed between 3000 and 6000 RPM can give good coating uniformity. For 4' wafer, 6000 RPM spinner speed was used to coat 3.2 um photoresist after experiments. AZ5214EZ is diluted with AZ1500 thinner (1:1) in order to get the thickness within the desired range.

Softbake can remove most of the remaining solvent from the photoresist film. AZ5214E resist is not very sensitive to light until its solvent component (propylene glycol monomethy ether acetate) is removed. Prebake is needed on hot plate to accelerate the solvent diffusion process before exposure. [14]. According to AZ5214E data sheet, temperatures above 100°C in an oven or 120°C on a hot plate will lead to reduced sensitivity and therefore can adversely affect process latitude. It's suggested that 90-110°C and 30-60seconds are appropriate for hot plate softbaking. After taking into consideration that lower softbake temperature will result in decreased adhesion and stability in later processing steps, we took 110°C for 45 seconds as softbake temperature, it can accelerate the solvent diffusion without lowering the resist photospeed [16].

Exposure will convert diazonaphthoquinone to indene carboxylic acid groups, which makes the film base soluble. PEB, flood exposure and development will give a negative image because liberated reactive agent. The exposure has a strong effect on the undercut profile because the image reversal process is simply reversing the original profile, it also has primary control of the linewidths. The photosensitivity of the AZ5200 photoresists in

positive tone is suitable for near *UV* (365-405 nm) exposure. These wavelengths can be used to achieve resolution of one micron and below in 1.5 micron thick resist films [16]. Actual exposure energies required will depend on film thickness, softbake conditions, spectral output of the exposure tool, and developing conditions. For our process of 4000 angstroms of resist, we need to optimize the exposure dose. Different level exposure intensity were performed by changing the exposure time from 0.05 second to 1 second by an increment of 0.05 second to see find a clearing dose for AZ5214 as positive resist, then that value will be the value below which we should use for image reversal process. The dose of energy in dimension of joules per square centimeter [J/cm^2] can be calculated by multiplying the illumination intensity that strikes the resist unit volume [W/cm^2] with the exposure time [s]. Underexposure will provide with lift-off profile. Overexposure will give positive profile sidewalls, which should be eliminated. Combining with experience from the RIT image reversal process and our film situation, a series of different set of exposure time and PEB temperature combination with the 436nm stepper system were tried to get the best process condition for lift-off.

Normally, a positive photoresist profile has a positive slope of 75 °C-85 °C depending on the process conditions and the performance of the exposure equipment. This is mainly due to the absorption of the PAC, which attenuates the light when penetrating through the resist layer (so called bulk effect) [13]. The result is a higher dissolution rate at the top and a lower rate at the bottom of the resist. When AZ 5214E is processed, the higher exposed areas will be crosslinked to a higher degree than those with lower dose and dissolution rates accordingly. The final result will be a negative wall profile [13].

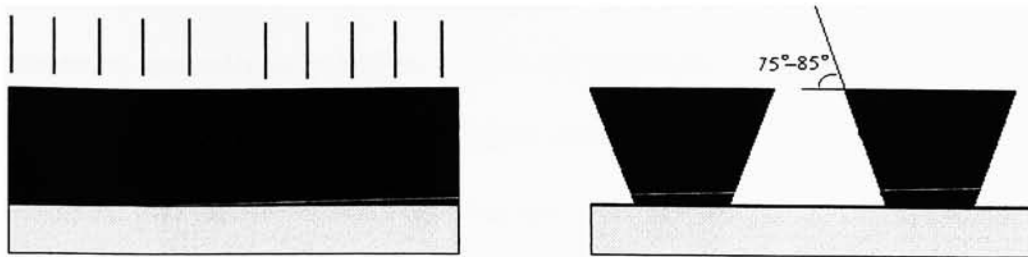

Figure 3.9 Cross section of photoresist profile during exposure and after development. Because of the bulk effect, the dissolution rate is higher at the top of exposed resist layer and lower at the bottom of the resist. Right: When AZ5214E is in Image Reversal mode, top area will be more crosslinked than the bottom area of resist, which means a negative profile.

The most critical parameter of the process is reversal-bake temperature, once optimized it must be kept constant within +/- 1° C to maintain a consistent process. In any case it will fall within the range from 115 to 125 ° C. If temperature is chosen too high (>130 ° C) the resist will thermally crosslink also in the unexposed areas, giving no pattern. To find out the suitable temperature following procedure is performed:

Coat and prebake substrates with resist. Without exposing them to *UV*, subject them to different reversal-bake temperatures, i.e. 115° C and 125° C. Apply a flood exposure of >200mj/cm^2 and immerse them into a standard developer, i.e. AZ 351B, 1:4 diluted, or AZ 726 MIF for 1 minute. On the substrates, where the resist will be removed, those exposed to a too high temperature will remain with the resist thermally crosslinked on it. The flood exposure is uncritical as long as sufficient energy is applied to make the unexposed areas soluble. 200 mj/cm^2 is a good choice, 150-500 mj/cm^2 will have no major influence on the performance.

It should be noted that the imagewise exposure energy is lower than with normal positive processes, generally only half of it. As a rule of thumb, compared to a standard positive resist process, imagewise exposure dose should be half of it, flood exposure energy double of that for AZ 5214E IR-processing [13]. We can see from SEM profile pictures of cross-section of imaged reversed resist for different process parameters, the 120° C/03second is the most effective image reversal parameter setup, by which we can see there is about 88 degree of negative profile.

AZ5200 series photoresists has high contrast in both inorganic and metal-ion-free developers [16]. We noted the following plasma thin film deposition demands the photoresist to be able to withstand higher temperature environments. The image stability during hard bake is dependent on the temperature and duration of the post exposure bake, with higher post exposure bake temperatures and times favoring greater thermal image stability. The thermal stability can be improved to 200° C with the image reversal mode of 120° C /0.3second [17]. After going through the image reversal and development process, a wafer was put into PVD system to go through the same plasma thermal process without any film deposition while being covered by a shield between plasma and wafer surface, the SEM picture clearly demonstrate the high degree of thermal image stability achieved by use of this image reversal process.

Figure 3.10 Cross-section profile after PVD thermal process

High contrast diluted developer offers the best contrast and resolution, while high sensitivity dilution allows shorter developing times or lower exposure doses. The specific dilution chosen will depend on the development time constraints and the desired image qualities. The developer should be maintained at a constant temperature (+/- 1°C) within the range of 20-25 °C [16]. We used the normal DI water diluted acetone (2:1) as developer. During developing, by orienting the sample properly, we see interference patterns fluctuate on the resist, first revealing the patterns and then making them disappear, and showing up again when the development progresses. Next, fluctuation ceases when the resist thickness becomes less than needed for interference in range of visible light. The first estimate for optimal development time is often taken by adding 15 seconds to the time needed to make the fluctuation to disappear [12]. By careful control and comparison, the best development condition is shipley Microposit 351 : DI water (1:6 ratio) in square glass dish (mix 100ml Microposit 351 with 600ml DI water) for approximately 35-40 seconds, actual clear should appear approximately 25 seconds, total development time should be less than 50 seconds, otherwise we would lose most of the resist across the wafer. Rinse the substrate immediately with DI water and then put in spin-dry-cleaner. Postbaking will generally improve image stability and adhesion as well as plasma and chemical resistance. Postbake up to 150°C for 30 minutes in a convection oven will result in only minor changes in resist profile.

Next, put wafers into PVD chamber to deposit *APSM* film. Then, develop to "lift-off" those unwanted films on the photoresist by acetone, Q-tip was used to accelerate the process by applying mechanical tangential force across the wafer surface. The *APSM* lift-

off would appear in 20 seconds and final structure be stabilized in 120 seconds. Wafers were cleaved through the structures for examination of critical dimension by SEM and microscope. The optimized lift-off process is shown by Table 3.4.

1	Prime wafers with HMDS on g-line wafer track~4000rpm / 45sec/105° C hot plate.
2	Manual spin-on coat resist ~ 6000*rpm* / 45sec
3	Prebake (soft bake) on hotplate ~ 110° C / 45sec
4	Image exposure by GCA stepper (g-line) ~ 0.3 sec (30mj/cm^2)
5	Post exposure bake (results in cross-linking) in exposed area~ 120° C / 90sec
6	Flood expose on kasper aligner (contact stepper)~20sec (400 mj/cm^2)
7	Develop in shipley Microposit 351 : DI water (1:6) in square glass dish for approximately 35-40 seconds, actual clearing should appear approximately 25 seconds, total development time should be less than 50 seconds.
8	Rinse immediately after develop, then go through spin-rinse-dryer (SRD).
9	Postbake on hotplate~120° C/2min.
10	APSM film deposition by PE 2400A system with Argon 30sccm and O_2 15 sccm at total power of 625 watts for 150 minutes at rotation speed of 2rpm. Targets are Al_2O_3 and *Nb* (Niobium). Final film thickness around 800A(angstrom).
11	Lift-Off development in acetone accompanied by scrubbing with Q-tip for about 140 seconds and then Spin-rinse-dry.
12	Critical dimension inspection.

Table 3.4. Lift-off procedures.

4. Results

4.1 Candidate films

4.1.1 *Al-NbO$_x$*

Upon our model of EMA thin film, we simulated the optical complex index when we combine these two separate materials into one single composite film. We can draw this conclusion that we are able to adjust the optical index of the composite thin film by adjusting the quantity of each individual material by adjusting the deposition condition.

Film Thickness	779 angstrom
Composite film optical constants	n=2.0198, k=0.344
Composite film transmittance at 157 nm	10.04%
Composite film reflectance at 157 nm	11.72%
Volume percentage of individual materials	Al_2O_3 84.5% and NbO_x 15.5%.

Table 4.1 EMA model prediction for *Al-NbO$_x$ APSM* film.

Based on these targets and our experimental parameters of each individual material, we can set up the deposition condition accordingly to manufacture films with this recipe.

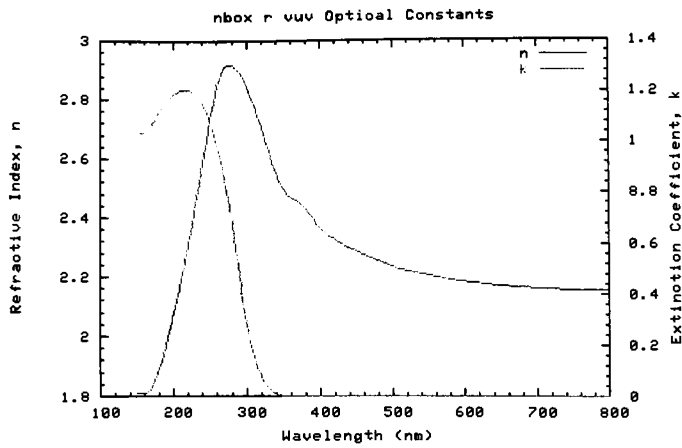

Figure 4.1 NbO_x complex index. Based on our pure NbO_x thin film, we derived its complex optical index VS. wavelength chart. The NbO_x thin film is deposited with power of 1000 watts and duration of 1 hour.

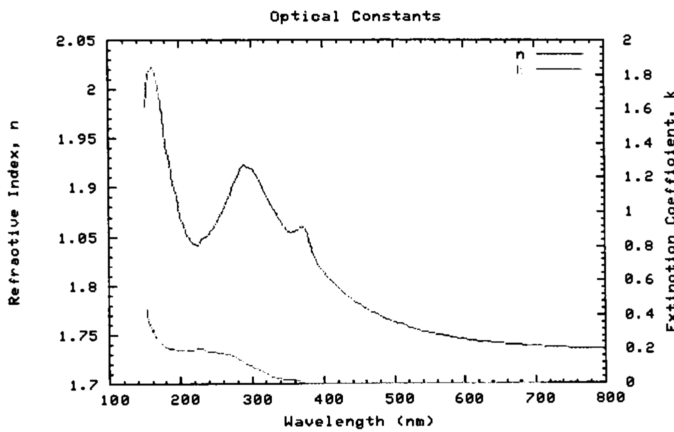

Figure 4.2 Al-NbO_x complex index from EMA model

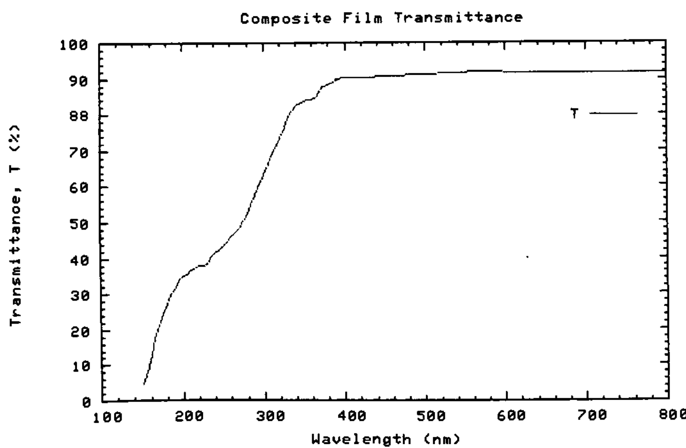

Figure 4.3 Transmission of Al-NbO_x thin film by simulation based on EMA model.
Also, we can simulate the final transmission of the composite Al-NbO_x thin film.

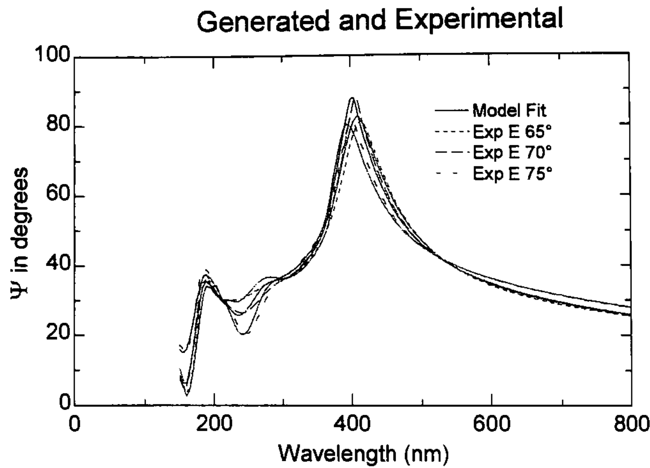

Figure 4.4 Al-NbOx complex index from measurement. MSE=23.08 for the real deposition *Al-NbOx* with thickness around 725.9A. The same as *Al-TaOx,* we optimize the deposition recipe, 7 minutes total power of 1250watts, 530voltages for *NbOx* target and 1720voltage for *Al_2O3* respectively.

But, from the measurement by *WVASE* ellipsometer, we can see the thickness is 725.9angstrom, which is much less than our theory model thickness of 779 angstroms.

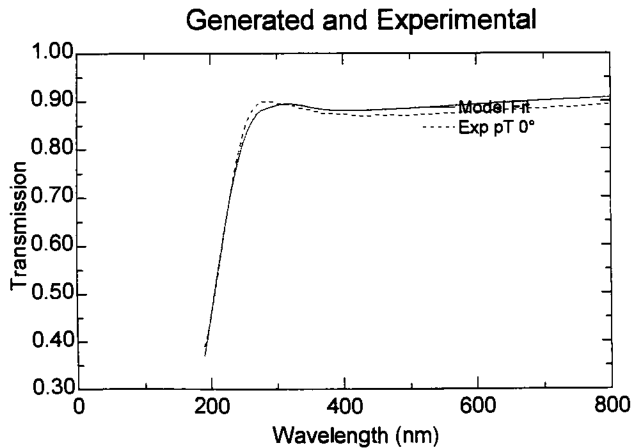

Figure 4.5 Comparison between modeling prediction and real transmission dispersion of Al-NbOx. Transmission VS wavelength for experimental *Al-NbOx* film, the transmission value is only available from 190nm and beyond because the substrate is not transparent under that value.

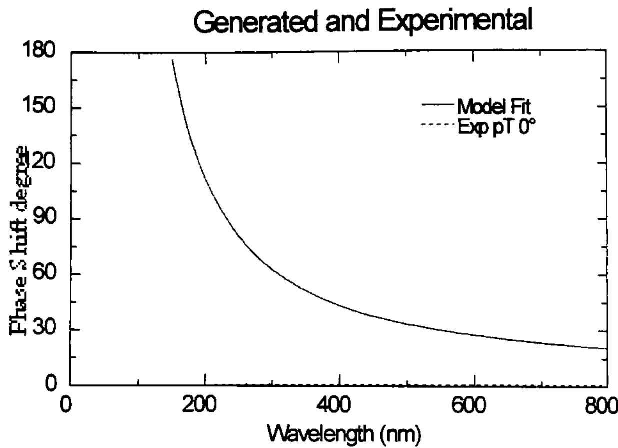

Figure 4.6 Phase shift dispersion chart for Al-NbOx film before thickness modification.

Phase shift VS wavelength for experimental *Al-NbOx* film, since the thickness of the film is much less than the target value, even the composition is correct, the phase shift value for 157nm is still out of acceptable error level, so corresponding correction is needed. Intentionally change to the right thickness, 790 A of the *APSM* film to get exactly 180 degree phase shift. The *WVASE* analysis software has the power to do the adjustment by simulation by changing the thickness to the right one and keeping the same optical property, by which we can predict the relative phase shift at that thickness and corresponding transmission.

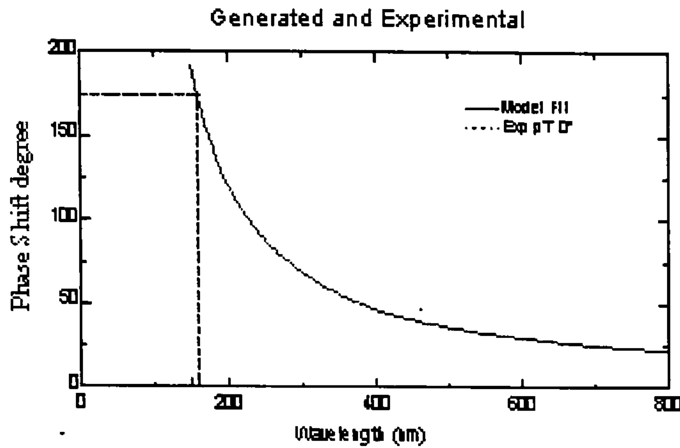

Figure 4.7 Phase shift for Al-NbOx film after thickness modification.

Phase shift vs. wavelength after change of the thickness to 790angstroms or *Al-NbOx* film, about 175°, which is within the acceptable error range.

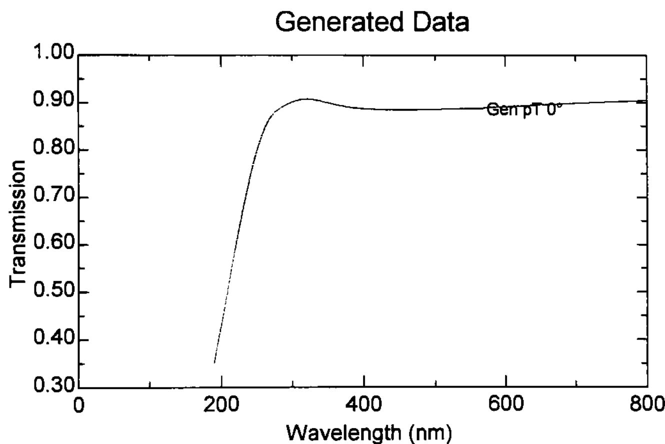

Figure 4.8 Transmission dispersion chart for Al-NbOx

Transmission vs wavelength for simulated *Al-NbOx* film after thickness change to 790 angstroms, the transmission value is only available from 190nm and beyond because the substrate is not transparent under that value. By doing this simulated change, we can keep the same optical property once they match our theory value and adjust the thickness

without physically doing it, by which can save a lot of time and still get the same good results.

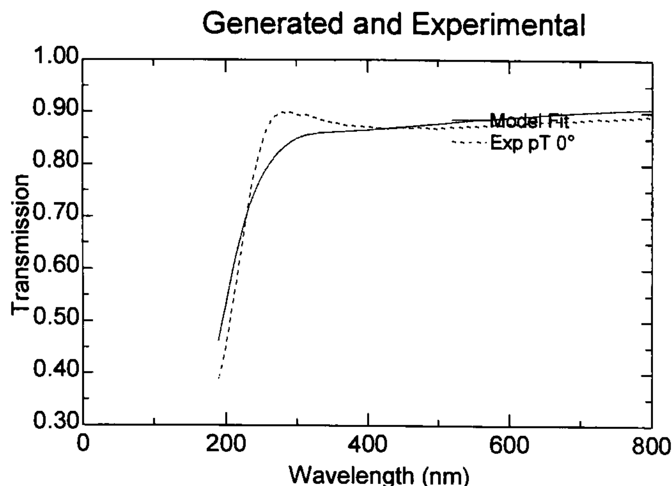

Figure 4.9 Comparison between EMA model generated data and real data for transmission dispersion. For the thickness of exactly 180 degree phase shift, we can simulate the corresponding transmission of the *APSM* film.

The EMA model of *WVASE* combines the constituent materials in the database to generate simulated transmission to compare with the real measured transmission data to confirm our model. In this case, we can see they also match very well.

Film thickness/phase shift	790 angstrom with175^{o} phase shift.
Composite film optical constants	n=2.01, k=0.33
Composite film transmittance at 157	11.6%
Composite film reflectance at 157 nm	12.31%
Volume percentage, Al_2O_3	84.5%
Volume percentage, NbO_x	15.5%.
Deposition time	67 minutes
Total power	1250watts
Power distribution	530voltages for *NbOx*/1720voltage

Table 4.2 *Al-NbOx* fabrication parameter and characteristics

4.1.2 *Al-TaO*$_x$

Upon our model of EMA thin film, we can simulate the optical complex index when we combine these two separate materials into one single composite film. We can see the final optical index is different from both of the parent materials, but fall kind of in between of them. We can draw this conclusion that we can adjust the optical index of the composite thin film by adjusting the quantity of each individual material by adjusting the deposition condition.

Film Thickness	782 angstrom
Composite film optical constants	n=2.0159, k=0.3248
Composite film transmittance at 157 nm	10.08%
Composite film reflectance at 157 nm	11.67%
Volume percentage of individual materials	Al_2O_3 91.3% and TaO_x 8.7%.

Table 4.3 EMA model prediction for $Al\text{-}TaO_x$ *APSM* film. Based on these targets and our experimental parameters of each individual material, we can set up the deposition condition accordingly to manufacture films with this recipe.

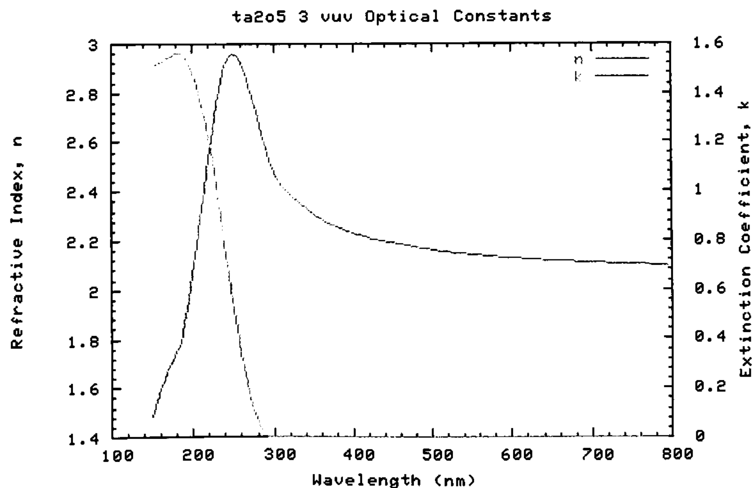

Figure 4.10 TaO_x complex index from EMA model.

Based on our pure TaO_x thin film, we derived its complex optical index VS. wavelength chart. The TaO_x thin film is deposited with power of 1000 watts and duration of 1 hour.

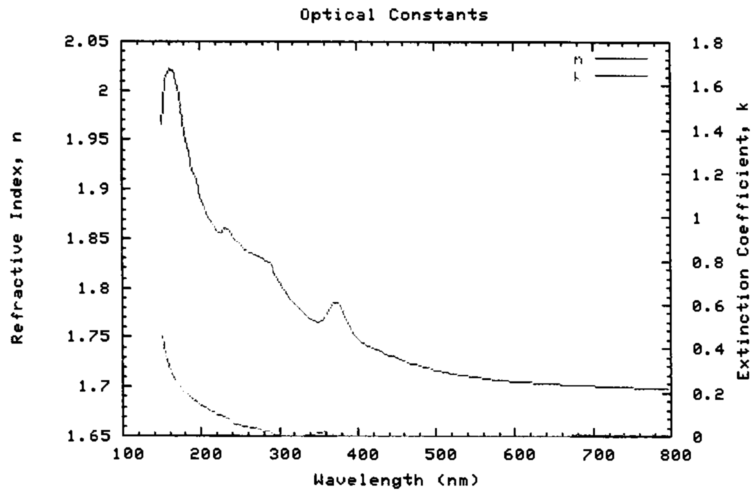

Figure 4.11 Al_2O_3 complex index from EMA model.

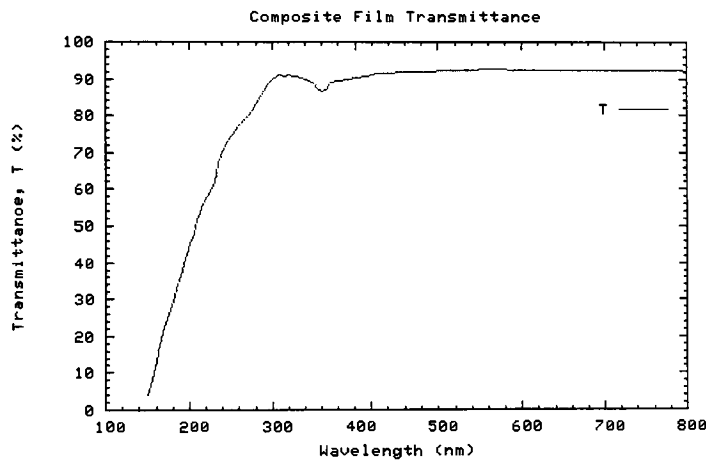

Figure 4.12 Transmission of $Al\text{-}TaO_x$ thin film by simulation based on EMA model The simulation is based on data from ellipsometer measurement and calculated with model predicted parameters.

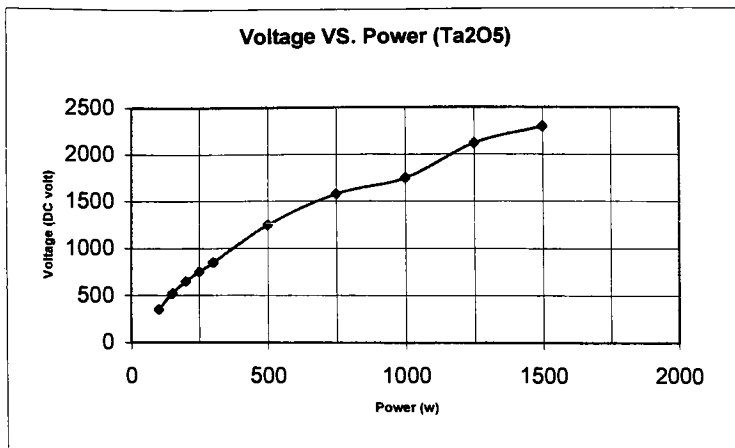

Figure 4.13 Voltage VS. Power for TaO_x

This chart describes the relationship between DC voltage bias on the target and the actual power supplied during deposition for single *Ta* target, which is useful later when we deposit multiple targets at the same time because we can monitor the voltage, which can be related to power and the deposition rate and composition control.

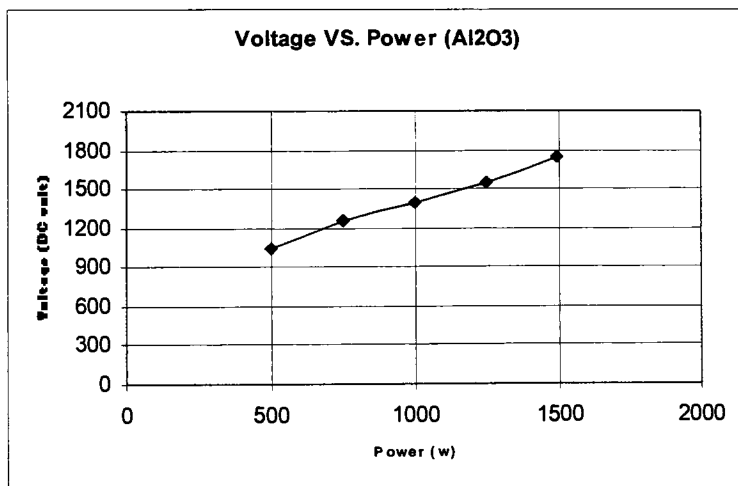

Figure 4.14 Voltage VS. Power for Al_2O_3

This chart describes the relationship between DC voltage bias on the target and the actual power supplied during deposition for single Al_2O_3 target, which is useful later when we

deposit multiple targets at the same time because we can monitor the voltage, which can be related to power and the deposition rate and composition control.

The configuration of our PVD system includes total power control, which can tell us the actual power being used on both targets when doing multi target deposition or total power on any single target when only using one of the three possible targets.

We can use at most two of the three targets to deposit composite films, and also the two targets must be at poison of 9 and 3 o'clock position. We can control the total power applied to the two targets combined. Also, we can distribute power between these two targets by control the DC biased voltage on each target, which can be read on their separate voltage meter. By doing this, we can realize different recipe by apply different power to each target, as their deposition rate is different under same or different power. For example of *Al-TaOx* APSM thin film, by volume percentage, Al_2O_3 should be around 91.3% and TaO_x 8.7%. To give a Pi phase shift of the incoming 157nm, the thickness of the final film should be around: 782 angstrom from calculation of our modeling. As a rule of thumb, the power is approximately proportional to deposition rate.
From our experiment, we know each individual deposition rate.

PVD condition	Deposition rate (*A*/min)
TaO_x at 1000w	4.5
Al_2O_3 at 1000w	11.3

Table 4.4 comparison of Al_2O_3 and TaO_x deposition rate.

Total power should not be too high considering the temperature problem related to later lift-off process to pattern the *APSM* film. We tried different powers and finalize at 1250watts, which can offer reasonable deposition rate also at relative lower working temperature.

Once the total power is set, we need to split the power to each targets, different set of combination were tried and the best is 1750V for Al_2O_3 and 300V for TaO_x.

PVD condition	Deposition rate (*A*/min)
TaO_x at 300V	1.13
Al_2O_3 at 1750V	6.75
$Al\text{-}TaO_x$ at 1250W	7.88
Time of deposition to achieve 782*A of* $Al\text{-}TaO_x$	
100min of total deposition time from calculation	

Table 4.5 $Al\text{-}TaO_x$ deposition parameter setup from calculation.

So, the deposition time is calculated by t=T/R, where t is the deposition time (min), T is the calculated thickness from theory and R is the deposition rate from experiment based on each individual targets.

The following is the modeling chart from *WVASE* software analysis of our actual $Al\text{-}TaO_x$ film, we can see the thickness is about 795 angstrom, which matches our prediction very well. Also, we can see how good the Model agree with the experimental data, the data was collected from three angles(65, 70, 75° respectively) of reflection which offers more information about the film and also the analysis will be more accurate and reliable.

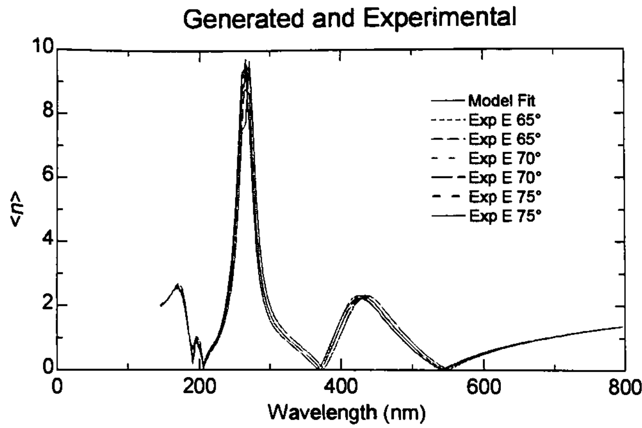

Figure 4.15 Ellipsometry analysis software fit chart for fabricated *Al-TaO*$_x$ thim film

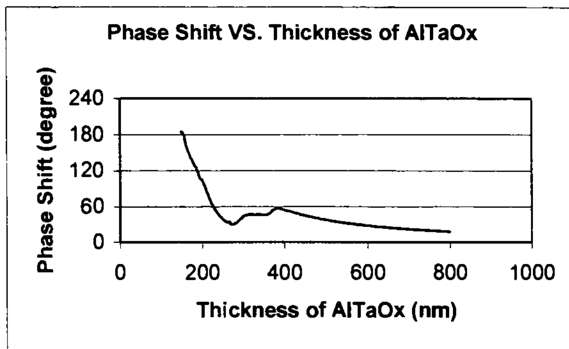

Figure 4.16 Phase shift dispersion chart for *Al-NbOx* film

We can see the phase shift chart measurement by the WVASE ellipsometer. At 157nm, the phase shift is about 179^0, which is within the phase error tolerable range (+/-5°).

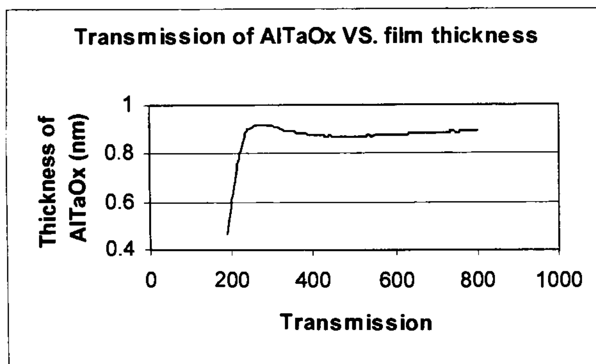

Figure 4.17 Transmission dispersion chart for *Al-TaOx*

Above is a chart of transmission dispersion curve for *Al-TaO*$_x$ film. The *WVASE* ellipsometer has wave ranges from 140 to 1800nm, but the substrate we use is high purity Silica, which is black below 190nm, so the curve only has a range from 190nm above. We can not check the transmission property at 157nm for *Al-TaO*$_x$. But, we can see the transmission property 40% transmission, which is good for mask inspection) at the inspecting wavelength, which is probably 193nm.

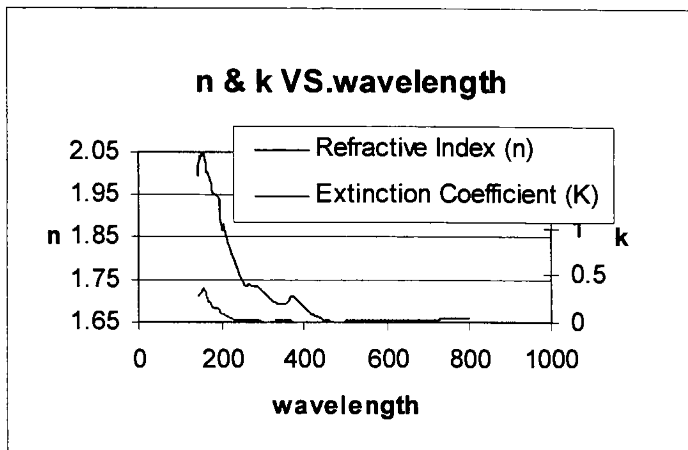

Figure 4.18 *Al-TaOx* complex index from measurement

Chart of complex optical index measured by *WVASE* ellipsometer, which matches our theory model very well.

Based upon above analysis and data, we can draw this conclusion that our theory model is accurate and reliable and we can predict the composite materials optical properties based on their constituent materials' optical properties. We can tailor the composition by adjust deposition parameters to get different thickness, different ratio of materials and finally different optical properties.

Film thickness/phase shift	795 angstrom with179^{0} phase shift.
Composite film optical constants	n=2.06, k=0.33
Composite film transmittance at 157	11.6%
Composite film reflectance at 157 nm	12.31%
Volume percentage, Al_2O_3	91.3%
Volume percentage, TaO_x	8.7%.
Deposition time	100 minutes
Total power	1250watts
Power distribution	300voltages for *NbOx*/1750voltage

Table 4.6 *Al-TaOx* fabrication parameter and characteristics.

4.1.3 ***Al-CrOx***

Upon our model of MEA thin film, we can simulate the optical complex index when we combine these two separate materials into one single composite film. We can see the final optical index is different from both of the parent materials, but fall kind of in between of them. We can draw this conclusion that we can adjust the optical index of the composite thin film by adjusting the quantity of each individual material by adjusting the deposition condition.

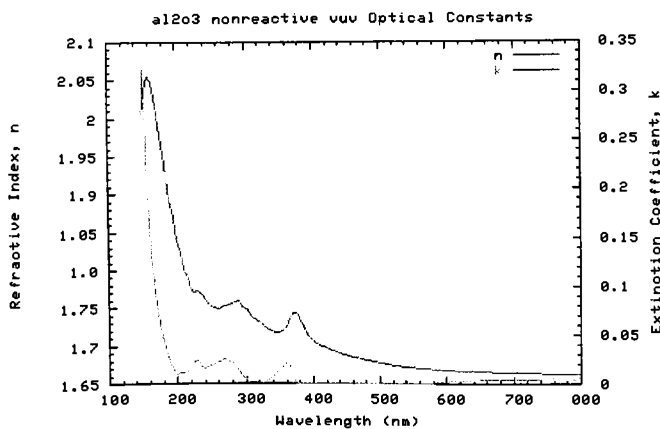

Figure 4.19 Al_2O_3 complex index from EMA model

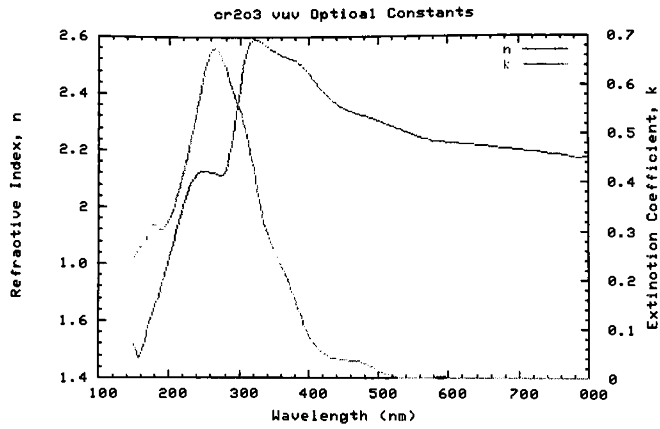

Figure 4.20 CrO_x complex index from EMA model

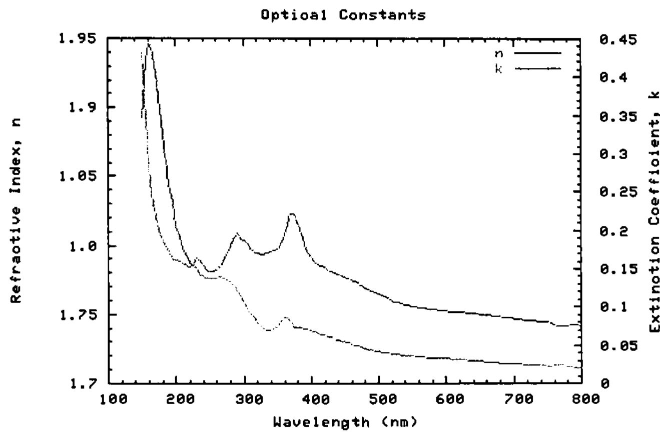

Figure 4.21 *Al-*CrO_x complex index from EMA model

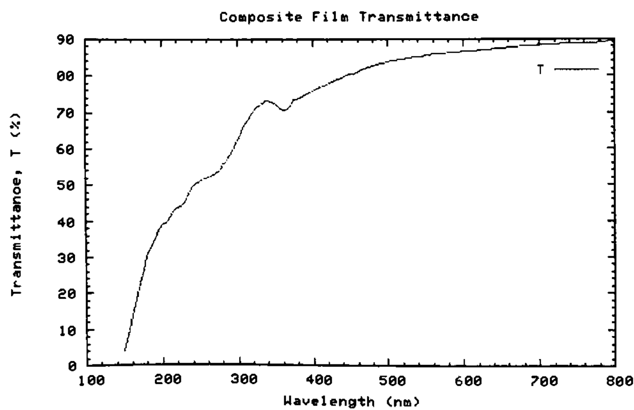

Figure 4.22 Transmission of *Al-*CrO_x thin film by simulation based on EMA model

Also, we can simulate the final transmission of the composite *Al-CrO$_x$* thin film.

Film Thickness	845 angstrom
Composite film optical constants	n=1.9390, k=0.3205
Composite film transmittance at 157 nm	10.04%
Composite film reflectance at 157 nm	10.92%
Volume percentage of individual materials	Al_2O_3 82.8% and CrO_x 17.2%.

Table 4.7 EMA model prediction for *Al-CrO$_x$ APSM* film.

Based on our pure Al_2O_3 thin film, we derived its complex optical index VS. wavelength chart. The Al_2O_3 thin film is deposited with power of 1000 watts and duration of 1 hour. Based on our pure Cr_2O_3 thin film, we derived its complex optical index VS. wavelength chart. The Cr_2O_3 thin film is deposited with power of 1000 watts and duration of 1 hour.

4.1.4 *Al-MoO$_x$*

Upon our model of MEA thin film, we can simulate the optical complex index when we combine these two separate materials into one single composite film. We can see the final optical index is different from both of the parent materials, but fall kind of in between of them. We can draw this conclusion that we can adjust the optical index of the composite thin film by adjusting the quantity of each individual material by adjusting the deposition condition.

Film Thickness	827 angstrom
Composite film optical constants	n=1.9594, k=0.3261
Composite film transmittance at 157 nm	10.07%
Composite film reflectance at 157 nm	11.11%
Volume percentage of individual materials	Al_2O_3 91.3% and MoO_x 8.7%.

Table 4.8 EMA model prediction for *Al-*MoO_x *APSM* film.

Based on these targets and our experimental parameters of each individual material, we can set up the deposition condition accordingly to manufacture films with this recipe.

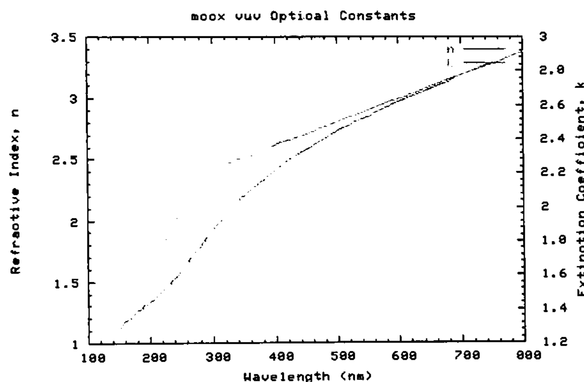

Figure 4.23 MoO_x complex index from EMA model

Based on our pure MoO_x thin film, we derived its complex optical index VS. wavelength chart. The MoO_x thin film is deposited with power of 1000 watts and duration of 1 hour.

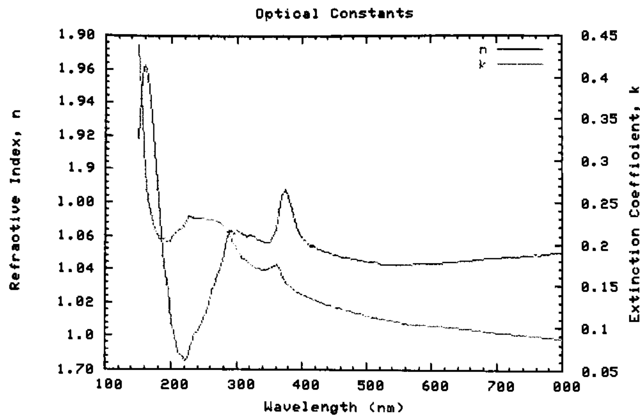

Figure 4.24 *Al-MoO$_x$* complex index from EMA model

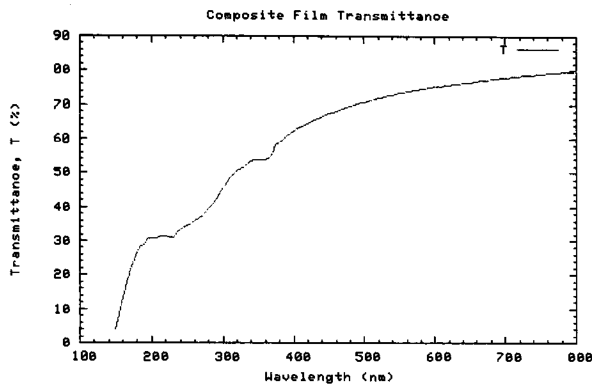

Figure 4.25 Transmission dispersion chart for *Al-MoO$_x$*

Also, we can simulate the final transmission of the composite *Al-MoO$_x$* thin film.

4.2 Lift-off

Different sets of experiments with various process parameters were tried and optimized to get best process condition for lift-off. It has demonstrated the image reversal technique is a repeatable and controllable process to liftoff *APSM* thin films with a critical dimension of two micron. The following is the corresponding SEM picture of the resist profile for different process conditions after Image reversal process and before film deposition process:

Figure 4.26 Condition.1: 115C° PEB/0.1 second of exposure

Figure 4.27 Condition.2: 125C° PEB/0.5 second of exposure

Figure 4.28 Condition.3: 120C° PEB/0.3 second of exposure

Figure 4.29 Condition.4: 120C° PEB/0.2 second of exposure

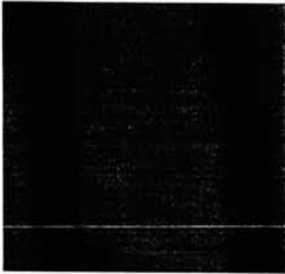

Figure 4.30 Condition.5: 115C° PEB/0.3 second of exposure

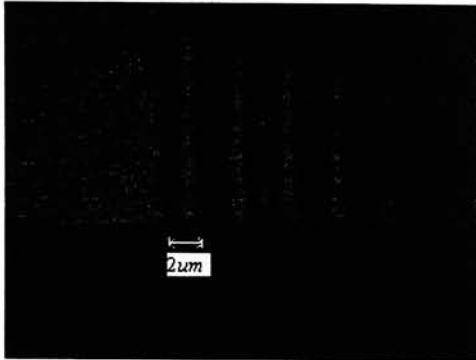

Figure 4.31 SEM picture of cleaved pattered *APSM* film by Image reversal process. The CD is 2*um*.

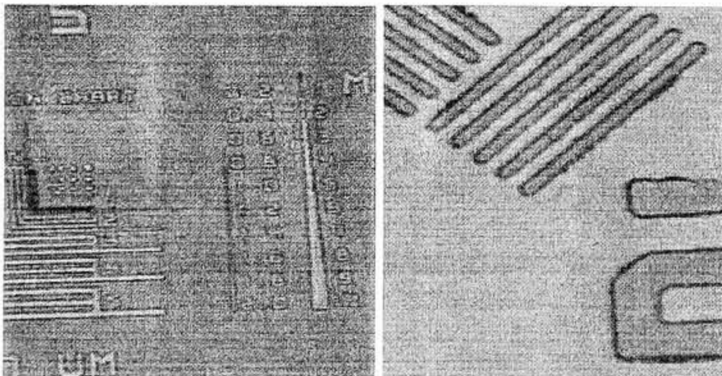

Figure 4.32Microscope picture of pattered *APSM* film by Image reversal process. The CD is 2 micron and even below as we can see from the CD marker.

The optimized process conditions were proved to be a reliable and repeatable lift-off process and be able to pattern our thin film materials with 2 micron CD. The details and discussion were listed in Table. 3.4 and experimental part of this thesis report.

5. Conclusion

As optical lithography, the major semiconductor industry enabler switching to 157 nm, materials issues will be more challenging. Most of the current thin film coatings may become inappropriate for shorter wavelength. New materials are needed for next generation wavelength node-157nm. The *APSM* should have transmission between 4% and 15% with a π phase shift for the transmitting working wavelength. And also the thin *APSM* film must be feasible to pattern. By carefully studying available materials optical properties derived from our research on PVD deposited thin films, no naturally occurred or stoichiometric materials can satisfy these requirements for *APSM* for 157nm.

So, non-stoichiometric composite materials were explored. In this case, the individual dielectric response of those constituents must be combined in an effective model to reproduce composite film dielectric response in terms of some wavelength independent parameters such as thickness and volume (or void) fractions. Models have been developed to describe the optical properties of dielectric, metallic, and composite film materials in interested wavelength regions. The relationships between thin film microstructure and optical properties are very useful for the development and characterization of thin films. The EMA theory will link thin film composition or microstructure to the spectral analysis of dielectric responses.

Al_2O_3.hosted composite materials are the most promising materials from our study. Four possible candidate (Al-NbO_x, Al-TaO_x Al-$CrOx$, Al-MoO_x) were suggested and modeled by our EMA method. Two (Al-NbO_x, Al-TaO_x) of them were fabricated according to our

model. Their optical properties satisfy the *APSM* requirements. Phase shift thickness for *Al-NbO*$_x$, is 790angstroms and give a real phase shift of 175^0 and transmission at possible inspection wavelength of 193nm is about 35%. The phase shift chart measurement by the WVASE ellipsometer points out the phase shift thickness of our *Al-TaO*$_x$, film is 785 angstroms and the phase shift is 179^0 with transmission at 193 nm of 45%. By adjusting the PVD deposition parameters, mainly reactive gas ratio, power on target materials, and power ratio of constituent materials of the composite films, we can modify the optical properties of *APSM* film by controlling the composition.

Secondly, the *Al-NbO*$_x$ film was patterned by image reversal lift-off process. The lift-off process is performed by AZ5214 resist, which is a positive resist but functions as a negative resist when combining with a post exposure bake. The following flood exposure will positively remove all of those unexposed area from previous step, this offers a negative profile after hard bake. The PVD *APSM Al-NbO*$_x$ film deposition gives a conformal film coverage, but interrupted by the negative sidewall slope. The final development lifts off the films in the unwanted areas because of the discontinued film coverage. It proves we can pattern the *Al-NbO*$_x$ film with a CD of 2 micron.

We can see by choosing the right materials and right combination, non-stoichiometric materials can be modeled correctly and fabricated accordingly to meet specific optical requirements. By strictly set up PVD process parameter, the composition and complex index of the composite films can be controlled and modified. Also a corresponding lift-off process was developed to pattern one (*Al-NbO*$_x$ film) of our candidate films with a

reasonable CD of 2 micron. *Al-NbO_x* film is one of the most promising candidate for *APSM* at 157nm, not only because its desirable optical property, also because it has more NbO_x by volume in the film. Since the deposition rate for NbO_x is higher than Al_2O_3, so that the total deposition time is shorter and cause less heat accumulation in the PVD chamber. Then less degradation for the AZ5214 resist and better patterning result for the lift-off process.

The work of this thesis offers a general approach for the 157nm *APSM* and a lift-off process to pattern the film. One can model the complex index of non-stoichiometric materials when the direct solution is not available; the model is based on our database of various materials' complex indexes. The fabrication process can be adjusted to suit for the optical requirements and the lift-off process is proved to be feasible to pattern the films.

6. References

1. Introduction to Microlithography, Bruce W. Smith, 1998.

2. Improving resolution in photolithography with a phase-shifting mask, Levenson, M. D., Viswanathan, N. S., and Simpson, IEEE Trans. Electron Devices, 1982.

3. Mutually optimizing resolution enhancement techniques: illumination, APSM, assist feature OPC, and gray bars, Bruce W. Smith, SPIE, 2001.

4. http://www.intel.com/research/silicon/mooreslaw.htm.

5. Patent No. US939227, Bruce W Smith, Multi-layered attenuated phase shift mask and a method for making the mask 1999.

6. Optical diagnostics for think film processing, Irving P. Herman

7. UV optical properties of thin films, Lena V. Zavyalova.

8. PVD & CVD process for coating tools, Rober Aharonov, IONBOND Corporation, Oct 17, 2000.

9. Milton Ohring, Materials Science of Thin Films, Academic Press, 2002

10. www.uiuc.edu/physics/lab , Physics Department, UIUC

11. Operation manual and instruction for WVASE, J.A. Woollam Corporation.

12. Lithography in experimental environment, Anssi Hovinen, Alexei Malinin, Antti Lipsanen, Reports in Electron Physics 2000/21 Espoo 2000.

13. AZ5214E positive photoresist for semiconductors and microelectronics, Hoechst Celanese Corporation data sheet, October 1985.

14. AZ5200 photoresists, Hoechst Celanese Corporation data sheet, February 1989.

15. "Lithographic process: the physics," in Introduction to Microlithography, L.F. Thompson and M.J. Bowden, American Chemical Society Symposium #219, 1983.

16. AZ 5200 positive photoresists, Hoechst Celanese Corporation data sheet.

17. Mechanism and lithographic evaluation of image reversal in AZ 5214 Photoresist, M. Spak, D. Mammato, S. Jaln, and D. Durham, American Hoechst Corporation, AZ Photoresist Products.

18. LOR lift-off Resists, MicroChem Corporation.

19. Advanced image reversal techniques, James W. Taylor, Thomas L. Brown, and David R. Bassett.

20. Attenuated phase shift mask materials for 248 and 193 nm lithography, B. W. Smith, S. Butt, Z. Alam, S. Kurinec and R. L. Lane.

21. Materials for attenuated phase shift Mask application at 193nm, Shahid Butt.

22. www.rit.edu/lithography, RIT lithography Group.

23. http://www.synopsys.com/products/ntimrg/subwave_chal_ds.html.

7. Abbreviations

APSM-attenuated phase shift mask
CD-critical dimension
CVD-chemical vapor deposition
DC-direct current
DI-distilled
DOF-depth of focus
EMA-effect media approximation
HMDS-hexamethyl disilazane
IC-integrated circuit
IR-infrared
k-absorption coefficient
n-refractive index
NA-numerical aperture
OAI-off-axis illumination
OPC-optical process correction
PAC-photo active compound
PSM-phase shift mask
PEB-post-exposure bake
PVD-physical vapor deposition
R-reflectance
R-resolution
RET-resolution enhancement technique
RF-radio frequency
RPM-rotation per minute
SCCM-standard cubic centimeter
SEM-scanning electron microscopy
T-transmission
UV-ultraviolet
VUV-vacuum ultraviolet